

Zero-field Time Correlation Functions of Four Classical Heisenberg Spins on a Ring

Richard A. Klemm^{1,2,3} and Marshall Luban²

¹*Max-Planck-Institut für Physik komplexer Systeme, Nöthnitzer Straße 38, D-01187 Dresden, Germany*

²*Ames Laboratory and Department of Physics and Astronomy, Iowa State University, Ames, IA 50011 USA*

³*Materials Science Division, Argonne National Laboratory, Argonne, IL 60439 USA*

(October 25, 2018)

A model relevant for the study of certain molecular magnets is the ring of $N = 4$ classical spins with equal near-neighbor isotropic Heisenberg exchange interactions. Assuming classical Heisenberg spin dynamics, we solve explicitly for the time evolution of each of the spins. Exact triple integral representations are derived for the auto, near-neighbor, and next-nearest-neighbor time correlation functions for any temperature. At infinite temperature, the correlation functions are reduced to quadrature. We then evaluate the Fourier transforms of these functions in closed form, which are double integrals. At low temperatures, the Fourier transform functions explicitly demonstrate the presence of magnons. Our exact results for the infinite temperature correlation functions in the long-time asymptotic limit differ qualitatively from those obtained assuming diffusive spin dynamics. Whether such explicitly non-hydrodynamic behavior would be maintained for large- N rings is discussed.

75.10.Hk,75.75.+a,75.30.Ds,75.75.-y

I. INTRODUCTION

Recently, there has been a rapidly growing interest in the physics of molecular magnets. [1,2] These compounds can be synthesized as single crystals of identical molecular units, each containing several paramagnetic ions that mutually interact via Heisenberg exchange. The intermolecular (dipole-dipole) magnetic interactions are in the great majority of cases utterly negligible as compared to intramolecular magnetic interactions. Measurements of the magnetic properties therefore reflect those of the common, individual molecular units of nanometer size. Their dynamics can be studied by inelastic neutron scattering, as well as by nuclear magnetic resonance and electron paramagnetic resonance experiments. Some of these molecular magnets are made of very small clusters of magnetic ions. The smallest clusters are dimers of V^{4+} ($S = 1/2$) and of Fe^{3+} ($S = 5/2$), [3,4] a nearly equilateral triangle array of V^{4+} spins, [5], a nearly square array of Nd^{3+} (total spin $j = 9/2$), [6] a regular tetrahedron of Cr^{3+} ($S = 3/2$), [7] a frustrated tetrahedral pyrochlore of Tb^{3+} ($S = 5/2$), [8] and a “squashed” tetrahedron of Fe^{3+} spins. [9,10] There has also been an example of a four-spin ring which is coupled to nearby rings, although the spin value ($S = 1/2$) is small, and thus requires a

quantum treatment. [11] In addition, larger rings, most notably with 6, 8, or 10 Fe^{3+} spins, have been studied. [12,13,14]

In some of these systems, the spin value of an individual magnetic ion is large enough that the dynamics can be closely approximated by the classical theory, as long as one does not go to temperatures that are too low. Thus, it is useful to study such systems theoretically, in order to investigate the types of dynamical spin behavior that can occur. Such investigations can provide helpful physical insight, as well as some guidance for systems that might be studied experimentally. It will also be interesting to compare the classical results with those emerging from studies of their quantum analogues, such as has been done for the dimer and the equilateral triangle. [15,16]

Perhaps more interesting, however, is the question as to whether the long-time asymptotic behavior of the two-spin correlation functions at infinite temperature will be consistent with the results of a hydrodynamic-like theory, in which the exact equations governing the spin dynamics are approximated by linear diffusion-like equations [see Eq. (84)]. This question has been the subject of much debate in the literature, [17,18,19,20], and a solution of the spin dynamics for the four-spin ring might aid in our understanding of this more fundamental problem. Here we derive exact results which explicitly demonstrate that the infinite temperature, long-time asymptotic limits of the $N = 4$ two-spin correlation functions are non-hydrodynamic.

The layout of the paper is as follows. In Sec. II, we give the notation, partition function, and derive the exact time evolution of the individual spin vectors. In Sec. III, we give the results for the time correlation functions. At infinite temperature, these results can be expressed as single integrals, but at finite temperatures, they are triple integrals. We also present our derivation of the Fourier transforms of the deviations of the correlation functions from their infinite time asymptotic limits. Finally, we invite the reader to read our discussion and conclusions in Sec. IV, even if one has only a minimal interest in the mathematical developments presented in Secs. II and III. In this final section, we also discuss the non-hydrodynamic aspects of our exact results for the infinite temperature, long-time asymptotic behaviors of the two-spin correlation functions, and raise the question as to whether such non-hydrodynamic features might be

maintained for larger rings.

II. SPIN DYNAMICS

A. Notation and partition function

We study the dynamics of four interacting spins on a ring. Each spin has unit magnitude and can assume an arbitrary direction. We suppose that it interacts only with its two nearest neighbors. We label these spins $\mathbf{S}_1, \mathbf{S}_2$, etc., where $|\mathbf{S}_i| = 1$, illustrated in Fig. 1.

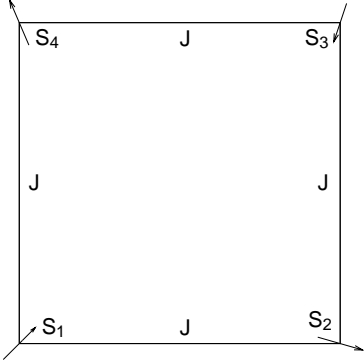


FIG. 1. Sketch of a ring with four classical spins at the corners, each interacting with its nearest neighbors with strength J .

The Hamiltonian for this system is thus

$$H = -J \sum_{i=1}^4 \mathbf{S}_i \cdot \mathbf{S}_{i+1}, \quad (1)$$

$$= -(J/2)(S^2 - S_{13}^2 - S_{24}^2), \quad (2)$$

where $\mathbf{S}_5 = \mathbf{S}_1$, $\mathbf{S}_{13} = \mathbf{S}_1 + \mathbf{S}_3$, $\mathbf{S}_{24} = \mathbf{S}_2 + \mathbf{S}_4$, and $\mathbf{S} = \mathbf{S}_{13} + \mathbf{S}_{24}$. [21]

The partition function Z can be readily found from Eq. (2), leading to

$$Z = \text{Tr} \exp(-\beta H) \quad (3)$$

$$\begin{aligned} &= \left(\prod_{i=1}^4 \int \frac{d\Omega_i}{4\pi} \right) \int d^3\mathbf{S} \int d^3\mathbf{S}_{13} \int d^3\mathbf{S}_{24} \times \\ &\quad \times \delta^{(3)}(\mathbf{S} - \mathbf{S}_{13} - \mathbf{S}_{24}) \delta^{(3)}(\mathbf{S}_{13} - \mathbf{S}_1 - \mathbf{S}_3) \times \\ &\quad \times \delta^{(3)}(\mathbf{S}_{24} - \mathbf{S}_2 - \mathbf{S}_4) \exp(-\beta H) \quad (4) \\ &= \left(\prod_{i=1}^4 \int \frac{d\Omega_i}{4\pi} \right) \int d^3\mathbf{S} \int d^3\mathbf{S}_{13} \int d^3\mathbf{S}_{24} \times \\ &\quad \times \int \frac{d^3\mathbf{k}}{(2\pi)^3} \int \frac{d^3\mathbf{p}}{(2\pi)^3} \int \frac{d^3\mathbf{q}}{(2\pi)^3} e^{i\mathbf{k} \cdot (\mathbf{S}_{24} - \mathbf{S}_2 - \mathbf{S}_4)} \times \\ &\quad \times e^{i\mathbf{p} \cdot (\mathbf{S}_{13} - \mathbf{S}_1 - \mathbf{S}_3)} e^{i\mathbf{q} \cdot (\mathbf{S} - \mathbf{S}_{13} - \mathbf{S}_{24})} e^{-\beta H} \end{aligned}$$

$$\begin{aligned} &= \left(\frac{2}{\pi} \right)^3 \int_0^\infty S^2 dS \int_0^\infty S_{13}^2 dS_{13} \int_0^\infty S_{24}^2 dS_{24} e^{-\beta H} \times \\ &\quad \times \int_0^\infty dk \frac{\sin^2 k \sin(kS_{24})}{kS_{24}} \int_0^\infty dp \frac{\sin^2 p \sin(pS_{13})}{pS_{13}} \times \\ &\quad \times \int_0^\infty dq \frac{\sin(qS) \sin(qS_{13}) \sin(qS_{24})}{qS S_{13} S_{24}} \\ &= \frac{1}{8} \int_0^2 dS_{13} \int_0^2 dS_{24} \int_{|S_{13}+S_{24}|}^{S_{13}+S_{24}} S dS e^{\alpha(S^2 - S_{13}^2 - S_{24}^2)}, \quad (5) \\ &= \frac{1}{8} \bar{Z}, \end{aligned}$$

where

$$\bar{Z} = \int_0^2 dx \frac{\cosh(4\alpha x) - 1}{2\alpha^2 x}, \quad (6)$$

and $\alpha = \beta J/2$. Eq. (6) was obtained previously, [21] and an analysis of the integral was also presented. The overall factor of $\frac{1}{8}$ can be dropped, as it will not appear in the correlation functions. In deriving Z , we note that the angles \mathbf{S}_{24} makes with \mathbf{k} and \mathbf{q} are independent, as are the angles \mathbf{S}_{13} makes with \mathbf{k} and \mathbf{p} . Hence, it is helpful to first integrate over the angles \mathbf{S}_1 and \mathbf{S}_3 make with \mathbf{p} and the angles \mathbf{S}_2 and \mathbf{S}_4 make with \mathbf{k} . Then, one may choose the coordinates of \mathbf{k} and \mathbf{p} relative to \mathbf{S}_{24} and \mathbf{S}_{13} , respectively.

B. Exact time evolution

The dynamics of the spins arise from the Heisenberg equations of motion,

$$\frac{d\mathbf{S}_i}{dt} = \frac{1}{\tau} \sum_{\substack{j=1 \\ \langle ij \rangle}}^N \mathbf{S}_i \times \mathbf{S}_j, \quad (7)$$

where $\mathbf{S}_{N+i} = \mathbf{S}_i$ for any integer i . Our primary concern in this paper is the case $N = 4$, for which Eq. (7) may be rewritten as

$$\frac{d\mathbf{S}_{1,3}}{dt} = \frac{1}{\tau} \mathbf{S}_{1,3} \times \mathbf{S}_{24}, \quad (8)$$

$$\frac{d\mathbf{S}_{2,4}}{dt} = \frac{1}{\tau} \mathbf{S}_{2,4} \times \mathbf{S}_{13} \quad (9)$$

which lead to

$$\frac{d\mathbf{S}_{13}}{dt} = \frac{1}{\tau} \mathbf{S}_{13} \times \mathbf{S}, \quad (10)$$

$$\frac{d\mathbf{S}_{24}}{dt} = \frac{1}{\tau} \mathbf{S}_{24} \times \mathbf{S}, \quad (11)$$

and

$$\frac{d\mathbf{S}}{dt} = 0. \quad (12)$$

The phenomenological classical spin precession rate $\frac{1}{\tau}$ can be obtained from first principles, starting from a

quantum Heisenberg model whose classical counterpart is given by the Hamiltonian in Eq. (1). In that case, one simply obtains $1/\tau = J/\hbar$. From Eq. (12) we see that the total spin \mathbf{S} is conserved during the dynamical development, and is thus constant both in magnitude and direction. Equations (10) and (11) are easily interpreted as describing the precession of the vectors \mathbf{S}_{13} and \mathbf{S}_{24} about the constant vector \mathbf{S} , keeping their lengths invariant. We note that Eqs. (8) and (9) show that each individual spin executes a more complicated dynamics, precessing about the particular \mathbf{S}_{13} or \mathbf{S}_{24} that describes the sum of its near-neighbor spins, which is itself precessing about the constant \mathbf{S} . From well-known examples of rigid-body dynamics, we thus expect that the motion of the individual spin vectors will feature two frequencies, one for precession about \mathbf{S} , and the other for precession about either $\mathbf{S} \pm \mathbf{S}_{24}$ or $\mathbf{S} \pm \mathbf{S}_{13}$, respectively.

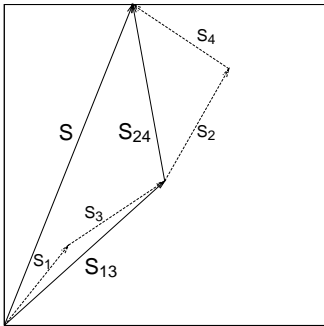


FIG. 2. Sketch of the spin vectors. \mathbf{S} , \mathbf{S}_{13} and \mathbf{S}_{24} all lie in a common plane where \mathbf{S}_{13} and \mathbf{S}_{24} each precess about \mathbf{S} . The unit vectors \mathbf{S}_1 and \mathbf{S}_3 initially point an arbitrary angle ϕ_{10} out of the plane, and precess about \mathbf{S}_{13} . Similarly, the unit vectors \mathbf{S}_2 and \mathbf{S}_4 initially point an arbitrary angle ϕ_{20} out of the plane, and precess about \mathbf{S}_{24} .

The conservation of \mathbf{S} enables us to solve Eqs. (10) and (11) exactly. Since $\mathbf{S} = \mathbf{S}_{13} + \mathbf{S}_{24}$ at all times, it is convenient to describe the motion in terms of the plane containing the three vectors \mathbf{S} , \mathbf{S}_{13} , and \mathbf{S}_{24} , as pictured in Fig. 2. We thus have

$$\mathbf{S}_{24}(t) = C_{24}\hat{\mathbf{s}} + A_{24}[\hat{\mathbf{x}} \cos(st/\tau) - \hat{\mathbf{y}} \sin(st/\tau)] \quad (13)$$

and

$$\mathbf{S}_{13}(t) = C_{13}\hat{\mathbf{s}} + A_{13}[\hat{\mathbf{x}} \cos(st/\tau) - \hat{\mathbf{y}} \sin(st/\tau)], \quad (14)$$

where $\hat{\mathbf{s}}$ is a unit vector parallel to \mathbf{S} , $\hat{\mathbf{x}}$ and $\hat{\mathbf{y}}$ are unit vectors normal to \mathbf{S} satisfying $\hat{\mathbf{x}} \times \hat{\mathbf{y}} = \hat{\mathbf{s}}$, thus completing the orthonormal basis set, and the constants A_{ij} and C_{ij} satisfy

$$A_{13}^2 + C_{13}^2 = S_{13}^2 \quad (15)$$

and

$$A_{24}^2 + C_{24}^2 = S_{24}^2. \quad (16)$$

We also have the relations

$$A_{24} = -A_{13} \quad (17)$$

and

$$C_{13} + C_{24} = S. \quad (18)$$

By combining Eqs. (15) and (18), we obtain

$$C_{13} = \frac{S^2 + S_{13}^2 - S_{24}^2}{2S} \quad (19)$$

and

$$C_{24} = \frac{S^2 + S_{24}^2 - S_{13}^2}{2S}. \quad (20)$$

We now determine the individual spin vectors \mathbf{S}_i . Because the four equations in Eqs. (8) and (9) have the same general structure, it suffices to focus on just one of them, say $\mathbf{S}_2(t)$. We write \mathbf{S}_2 in terms of its components, S_{2s} , S_{2x} , and S_{2y} , and make use of the standard Fourier transform $S_{2i}(t) = \int \frac{d\omega}{2\pi} \exp(i\omega t) S_{2i}(\omega)$. We also let $S_{2\pm} = S_{2x} \pm iS_{2y}$, and $\omega_{\pm} = \omega \pm S/\tau$. We then obtain

$$\omega S_{2s}(\omega) = \frac{A_{13}}{2\tau} [S_{2+}(\omega_-) - S_{2-}(\omega_+)] \quad (21)$$

and

$$\omega S_{2\pm}(\omega) = \mp \frac{C_{13}}{\tau} S_{2\pm}(\omega) \pm \frac{A_{13}}{\tau} S_{2s}(\omega_{\pm}). \quad (22)$$

Solving for $S_{2\pm}(\omega)$, and then replacing ω by ω_{\mp} , we have

$$S_{2\pm}(\omega_{\mp}) = \frac{A_{13} S_{2s}(\omega)}{C_{24} \pm \omega\tau}, \quad (23)$$

where we have employed Eq. (18). Solving for $S_{2s}(\omega)$, we then find

$$\frac{\omega}{C_{24}^2 - (\omega\tau)^2} (S_{24}^2 - (\omega\tau)^2) S_{2s}(\omega) = 0. \quad (24)$$

This implies that $S_{2s}(\omega)$ has components from three frequencies only, $\omega = 0, \pm S_{24}/\tau$. Thus, we write

$$S_{2s}(\omega) = 2\pi S_{2s0} \delta(\omega) + \pi \Delta S_{2s0} \left[e^{i\phi_{20}} \delta(\omega - S_{24}/\tau) + e^{-i\phi_{20}} \delta(\omega + S_{24}/\tau) \right], \quad (25)$$

or in real time,

$$S_{2s}(t) = S_{2s0} + \Delta S_{2s0} \cos(S_{24}t/\tau + \phi_{20}), \quad (26)$$

where the constants S_{2s0} and ΔS_{2s0} will be determined below, and ϕ_{20} is the arbitrary angle at which \mathbf{S}_2 initially makes with the Fig. 2. We note, however, that \mathbf{S}_4 must

make the same initial angle $\phi_{40} = \phi_{20}$ with this plane, since both spins have unit length, and their sum \mathbf{S}_{24} is contained within that plane. Analogously, \mathbf{S}_1 and \mathbf{S}_3 both make the arbitrary initial angle ϕ_{10} with that plane.

Combining Eqs. (23) and (25), we may solve for $S_{2\pm}(\omega)$,

$$S_{2\pm}(\omega) = \frac{2\pi A_{24} S_{2s0} \delta(\omega \pm S/\tau)}{C_{24}} + \pi A_{24} \Delta S_{2s0} \left(\frac{e^{\pm i\phi_{20}} \delta[\omega \pm (S - S_{24})/\tau]}{C_{24} - S_{24}} + e^{\mp i\phi_{20}} \frac{\delta[\omega \pm (S + S_{24})/\tau]}{C_{24} + S_{24}} \right). \quad (27)$$

Inverting the Fourier transform, and using $S_{2x} = (S_{2+} + S_{2-})/2$, $S_{2y} = (S_{2+} - S_{2-})/(2i)$, we have

$$S_{2x}(t) = \frac{A_{24}}{C_{24}} S_{2s0} \cos(St/\tau) + \frac{A_{24} \Delta S_{2s0}}{2[S_{24} + C_{24}]} \cos[(S + S_{24})t/\tau + \phi_{20}] - \frac{A_{24} \Delta S_{2s0}}{2[S_{24} - C_{24}]} \cos[(S - S_{24})t/\tau - \phi_{20}] \quad (28)$$

and

$$S_{2y}(t) = -\frac{A_{24} S_{2s0}}{C_{24}} \sin(St/\tau) - \frac{A_{24} \Delta S_{2s0}}{2[S_{24} + C_{24}]} \sin[(S + S_{24})t/\tau + \phi_{20}] + \frac{A_{24} \Delta S_{2s0}}{2[S_{24} - C_{24}]} \sin[(S - S_{24})t/\tau - \phi_{20}]. \quad (29)$$

Thus, as pictured in Fig. 2, \mathbf{S}_2 , and correspondingly, \mathbf{S}_4 , precesses about \mathbf{S}_{24} , which itself precesses about \mathbf{S} . As in Fig. 2, \mathbf{S}_1 and \mathbf{S}_3 each precesses about \mathbf{S}_{13} , which itself precesses about \mathbf{S} .

To evaluate the amplitudes S_{2s0} and ΔS_{2s0} , we use the fact that $S_{2\pm}^2(t) = 1$ to obtain

$$S_{24}^2 \left(\frac{S_{2s0}^2}{C_{24}^2} + \frac{(\Delta S_{2s0})^2}{A_{24}^2} \right) = 1, \quad (30)$$

which is independent of ϕ_{20} . This equation provides a constraint upon the two amplitudes S_{2s0} and ΔS_{2s0} . We may then immediately write down the analogous equation for the amplitudes S_{4s0} and ΔS_{4s0} appearing in the analogous expression for $\mathbf{S}_4(t)$,

$$S_{24}^2 \left(\frac{S_{4s0}^2}{C_{24}^2} + \frac{(\Delta S_{4s0})^2}{A_{24}^2} \right) = 1. \quad (31)$$

Since $\mathbf{S}_4(t) = \mathbf{S}_{24}(t) - \mathbf{S}_2(t)$, where $\mathbf{S}_{24}(t)$ is given in Eq. (13), the expressions for $\mathbf{S}_2(t)$ given by Eqs. (26), (28), and (29), and the analogous ones for $\mathbf{S}_4(t)$ (with S_{2s0} and ΔS_{2s0} replaced by S_{4s0} and ΔS_{4s0} , respectively) are consistent, provided that

$$S_{4s0} = C_{24} - S_{2s0} \quad (32)$$

and

$$\Delta S_{4s0} = -\Delta S_{2s0}. \quad (33)$$

Substituting Eqs. (32) and (33) into Eq. (31), and subtracting the results from Eq. (30), we have

$$S_{2s0} = S_{4s0} = C_{24}/2. \quad (34)$$

Then, from Eq. (30), we find

$$\Delta S_{2s0} = -\Delta S_{4s0} = \frac{A_{24}}{S_{24}} [1 - S_{24}^2/4]^{1/2}. \quad (35)$$

In Eq. (35), we have made the arbitrary choice of assigning the positive sign to ΔS_{2s0} , but that does not affect any of the results. Thus, we have now completely determined the dynamics of $\mathbf{S}_2(t)$ and $\mathbf{S}_4(t)$, except for the arbitrary phase ϕ_{20} representing the angle that $\mathbf{S}_2(0)$ makes with the plane containing \mathbf{S} , \mathbf{S}_{24} , and \mathbf{S}_{13} . Similarly, $\mathbf{S}_1(t)$ is obtained from Eqs. (26), (28), (29), (34), and (35) by replacing A_{24} , C_{24} , S_{24} , and ϕ_{20} with A_{13} , C_{13} , S_{13} , and ϕ_{10} , respectively. $\mathbf{S}_3(t)$ is then obtained from $\mathbf{S}_1(t)$ in the same way as $\mathbf{S}_4(t)$ was obtained from $\mathbf{S}_2(t)$.

III. TIME CORRELATION FUNCTIONS

In this section, we utilize the exact results for the dynamics of the four spin vectors derived in the previous section to obtain analytical formulas for the three distinct time correlation functions.

A. General Results

There are three inequivalent correlation functions, which we denote by $\mathcal{C}_{22}(t) = \langle \mathbf{S}_2(t) \cdot \mathbf{S}_2(0) \rangle$, $\mathcal{C}_{12}(t) = \langle \mathbf{S}_1(t) \cdot \mathbf{S}_2(0) \rangle$, and $\mathcal{C}_{24}(t) = \langle \mathbf{S}_2(t) \cdot \mathbf{S}_4(0) \rangle$, where $\langle \dots \rangle = \text{Tr}[\exp(-\beta H) \dots] / Z$. These are the spin-spin autocorrelation function, the near-neighbor spin-spin correlation function, and the next-nearest-neighbor spin-spin correlation function, respectively. In evaluating these functions, we must average over the initial conditions, which means not only the averages over S , S_{24} , and S_{13} , but also over the initial angles ϕ_{10} and ϕ_{20} , which are present in Eq. (4) in the integrations over the solid angles Ω_1 and Ω_2 . We note that all of the correlation functions depend upon the temperature through the parameter α , but to keep the notation simple, we suppress that dependence. The simplest of these $\mathcal{C}_{ij}(t)$ is $\mathcal{C}_{12}(t)$, for which the independent averages over ϕ_{10} and ϕ_{20} greatly simplify the final expression. We find

$$\begin{aligned}
\mathcal{C}_{12}(t) &= \frac{1}{4} \langle C_{13}C_{24} + A_{13}A_{24} \cos(St/\tau) \rangle \quad (36) \\
&= \frac{1}{4\bar{Z}} \int_0^2 dx \int_0^2 dy \int_{|x-y|}^{x+y} s ds e^{\alpha(s^2-x^2-y^2)} \times \\
&\quad \left[\frac{s^4 - (x^2 - y^2)^2}{4s^2} \right. \\
&\quad \left. - \left(y^2 - \frac{[s^4 + (x^2 - y^2)^2]}{4s^2} \right) \cos(st/\tau) \right], \quad (37)
\end{aligned}$$

where $\alpha = \beta J/2$, \bar{Z} is given by Eq. (6), and we have replaced S , S_{13} , and S_{24} by s , x , and y , respectively. After some algebra, the autocorrelation function is found to be

$$\mathcal{C}_{22}(t) = I_0 + I_1(t) + I_2(t) + I_3(t), \quad (38)$$

where

$$I_0 = \frac{1}{4} \langle C_{24}^2 \rangle, \quad (39)$$

$$I_1(t) = \frac{1}{4} \langle A_{24}^2 \cos(St/\tau) \rangle, \quad (40)$$

$$I_2(t) = \frac{1}{2} \langle \frac{A_{24}^2}{S_{24}^2} [1 - S_{24}^2/4] \cos(S_{24}t/\tau) \rangle, \quad (41)$$

and

$$\begin{aligned}
I_3(t) &= \frac{1}{2} \langle \frac{[1 - S_{24}^2/4]}{S_{24}^2} \left([C_{24}^2 + S_{24}^2] \times \right. \\
&\quad \times \cos(St/\tau) \cos(S_{24}t/\tau) \\
&\quad \left. + 2C_{24}S_{24} \sin(St/\tau) \sin(S_{24}t/\tau) \right) \rangle. \quad (42)
\end{aligned}$$

Using the same notation as in Eq. (37), we have

$$\begin{aligned}
I_0 &= \frac{1}{4\bar{Z}} \int_0^2 dx \int_0^2 dy \int_{|x-y|}^{x+y} s ds \times \\
&\quad \times e^{\alpha(s^2-x^2-y^2)} \frac{(s^2 - x^2 + y^2)^2}{4s^2}, \quad (43)
\end{aligned}$$

$$\begin{aligned}
I_1(t) &= \frac{1}{4\bar{Z}} \int_0^2 dx \int_0^2 dy \int_{|x-y|}^{x+y} s ds e^{\alpha(s^2-x^2-y^2)} \times \\
&\quad \times \cos(st/\tau) \left(y^2 - \frac{(s^2 - x^2 + y^2)^2}{4s^2} \right), \quad (44)
\end{aligned}$$

$$\begin{aligned}
I_2(t) &= \frac{1}{2\bar{Z}} \int_0^2 dx \int_0^2 dy \frac{(1 - y^2/4)}{y^2} \cos(yt/\tau) \times \\
&\quad \times \int_{|x-y|}^{x+y} s ds e^{\alpha(s^2-x^2-y^2)} \times \\
&\quad \times \left(y^2 - \frac{(s^2 - x^2 + y^2)^2}{4s^2} \right), \quad (45)
\end{aligned}$$

and

$$\begin{aligned}
I_3(t) &= \frac{1}{2\bar{Z}} \int_0^2 dx \int_0^2 dy \frac{(1 - y^2/4)}{y^2} \int_{|x-y|}^{x+y} s ds \times \\
&\quad \times e^{\alpha(s^2-x^2-y^2)} \left[\left(y^2 + \frac{(s^2 - x^2 + y^2)^2}{4s^2} \right) \times \right.
\end{aligned}$$

$$\begin{aligned}
&\quad \times \cos(yt/\tau) \cos(st/\tau) \\
&\quad \left. + \frac{y(s^2 - x^2 + y^2)}{s} \sin(st/\tau) \sin(yt/\tau) \right]. \quad (46)
\end{aligned}$$

Finally, $\mathcal{C}_{24}(t)$ may be found from

$$\langle \mathbf{S}_{24}(t) \cdot \mathbf{S}_{24}(0) \rangle = 2\mathcal{C}_{22}(t) + 2\mathcal{C}_{24}(t), \quad (47)$$

or

$$\begin{aligned}
\mathcal{C}_{24}(t) &= -\mathcal{C}_{22}(t) + \frac{1}{2} \langle C_{24}^2 + A_{24}^2 \cos(St/\tau) \rangle \\
&= 2I_0 + 2I_1(t) - \mathcal{C}_{22}(t) \\
&= I_0 + I_1(t) - I_2(t) - I_3(t). \quad (48)
\end{aligned}$$

By interchanging the integrations over x and y , it is easy to see that $\langle C_{13}C_{24} \rangle = \langle S^2/2 - C_{24}^2 \rangle$. Thus, we note that $\mathcal{C}_{12}(t)$ is equivalent to

$$\mathcal{C}_{12}(t) = \langle S^2 \rangle / 8 - I_0 - I_1(t). \quad (49)$$

We therefore remark that the $\mathcal{C}_{ij}(t)$ satisfy the conservation law,

$$\mathcal{C}_{22}(t) + \mathcal{C}_{24}(t) + 2\mathcal{C}_{12}(t) = \langle \mathbf{S}(t) \cdot \mathbf{S}(0) \rangle / 4 = \langle S^2 \rangle / 4, \quad (50)$$

a temperature-dependent quantity. Hence, in the infinite time limit, two of the three correlation functions $\mathcal{C}_{ij}(t)$ approach the same limit,

$$\lim_{t \rightarrow \infty} \mathcal{C}_{22}(t) = \lim_{t \rightarrow \infty} \mathcal{C}_{24}(t) = I_0, \quad (51)$$

but

$$\lim_{t \rightarrow \infty} \mathcal{C}_{12}(t) = \langle S^2 \rangle / 8 - I_0, \quad (52)$$

since the other terms vanish due to the infinite number of oscillations of the integrand within the interval of integration. This is essentially a consequence of angular momentum conservation. [22]

B. Reduction to Quadrature at Infinite Temperature

1. Analytic results at infinite temperature and time

In the limits $t, T \rightarrow \infty$, we can evaluate the $\mathcal{C}_{ij}(t)$ analytically. From Eqs. (38), (48), and (49), we note that these three functions are all given by the $T \rightarrow \infty$ limit of I_0 and the $I_i(t)$ for $i = 1, 2$, and 3. We first consider the simplest of these, I_0 , which gives the $t \rightarrow \infty$ limit. We find,

$$\lim_{\substack{t \rightarrow \infty \\ T \rightarrow \infty}} \mathcal{C}_{22}(t) = \lim_{\substack{t \rightarrow \infty \\ T \rightarrow \infty}} \mathcal{C}_{24}(t) = \frac{1}{4} + \delta_4 \quad (53)$$

and

$$\lim_{\substack{t \rightarrow \infty \\ T \rightarrow \infty}} \mathcal{C}_{12}(t) = \frac{1}{4} - \delta_4, \quad (54)$$

where

$$\delta_4 = \frac{8}{45} \ln 2 - \frac{11}{180} \approx 0.062115. \quad (55)$$

At first sight, one might have intuitively expected that the three $\mathcal{C}_{ij}(t)$ should be equal to each other as $t, T \rightarrow \infty$, and since $\lim_{T \rightarrow \infty} \langle S^2 \rangle / 4 = 1$, Eq. (50) would require each of them to equal $1/4$. This expectation is in fact the result predicted by conventional diffusive spin dynamics in the infinite temperature limit. [23] Moreover, for finite times that formalism predicts that all of the correlation functions depart from their common infinite-time limit by terms that decay exponentially to zero. However, our present rigorous results, Eqs. (53) - (55), as well as (59) - (61) in the following, show that these expectations are without foundation. Similar findings apply for the following simpler systems: the classical dimer, equilateral triangle, and regular tetrahedron, [23], for which the exact time correlation functions are derived as one-dimensional integrals for all times and temperatures.

2. One-dimensional integral representations

In this subsection, we give one-dimensional integral representations for the three time correlation functions at infinite temperature. One important advantage of these reduced forms is that they allow us to easily derive analytical formulas for the leading corrections to the long-time asymptotic values for finite times of each of the correlation functions. Another important advantage is that it becomes possible to obtain extremely accurate numerical values for the infinite temperature correlation functions for all times. By comparison, for finite temperature, accurate numerical evaluation of the three-dimensional integrals in Eqs. (43) - (46) becomes a major challenge.

We have found that the three functions $I_i(t)$ may be written as

$$\begin{aligned} \lim_{T \rightarrow \infty} I_1(t) &= \int_0^2 ds f_1(s) \cos(st^*) \\ &\quad + \int_2^4 ds g_1(s) \cos(st^*), \\ \lim_{T \rightarrow \infty} I_2(t) &= \int_0^2 ds f_2(s) \cos(st^*), \end{aligned} \quad (57)$$

and

$$\begin{aligned} \lim_{T \rightarrow \infty} I_3(t) &= \int_0^2 ds f_3(s) \cos(st^*) \\ &\quad + \int_2^4 ds g_3(s) \cos(st^*) \end{aligned}$$

$$+ \int_4^6 ds h_3(s) \cos(st^*), \quad (58)$$

where $t^* = t/\tau$, and analytic forms for the $f_i(s)$, $g_i(s)$ and $h_3(s)$ are listed in the Appendix. The infinite temperature correlation functions $\mathcal{C}_{22}(t)$, $\mathcal{C}_{24}(t)$, and $\mathcal{C}_{12}(t)$ are then simply found using Eqs. (38), (48), and (49), respectively. Thus, we have reduced these infinite temperature correlation functions to quadrature. They are shown for $0 \leq t/\tau \leq 10$ in Fig. 3a.

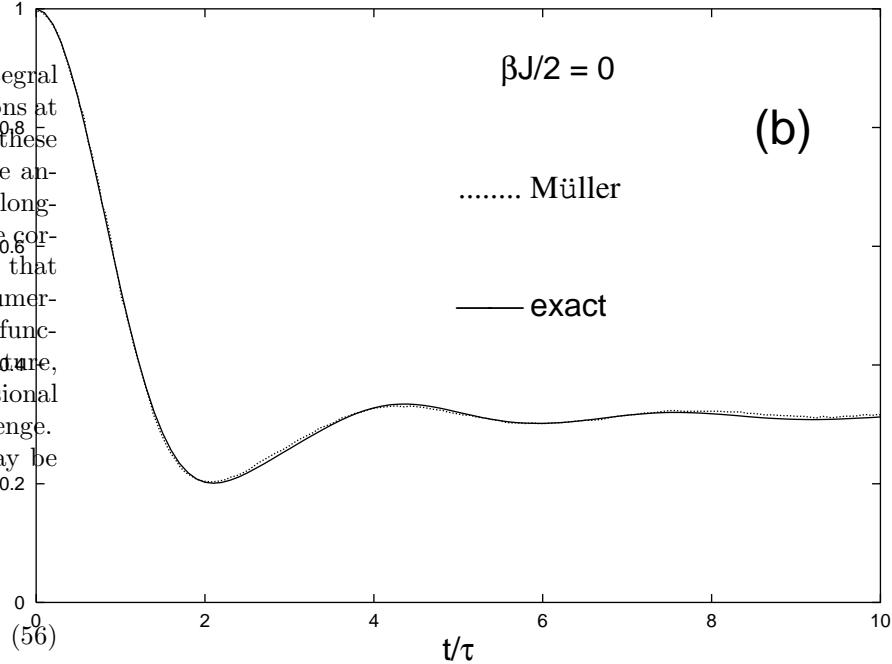
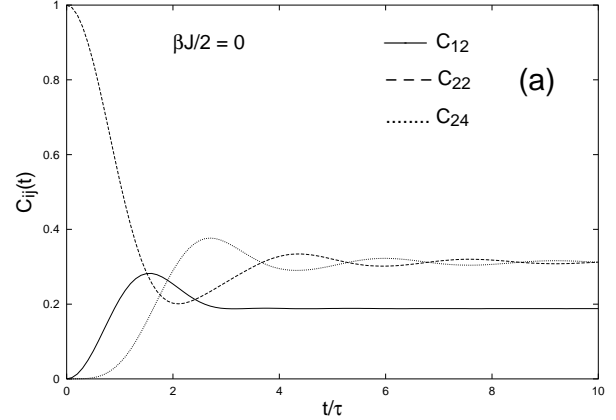


FIG. 3. (a) Plot of $\mathcal{C}_{12}(t)$ (solid), $\mathcal{C}_{24}(t)$ (dotted), and $\mathcal{C}_{22}(t)$ (dashed) versus t/τ in the infinite temperature limit $\alpha = 0$. (b) Comparison of the numerical results of Müller [17] (dashed) with our exact results (solid) for the infinite temperature ($\alpha = 0$) autocorrelation function $\mathcal{C}_{22}(t)$.

We remark that the infinite temperature autocorrelation function $\mathcal{C}_{22}(t)$ was obtained previously using a purely numerical procedure. [17] In Fig. 3b, we have

compared those published results with our exact formula at infinite temperature. Although there was some distortion in the axes in the published figure, using a pure rotation to account for this distortion led to the excellent agreement between the numerical and exact results.

From Fig. 3a, the autocorrelation function $C_{22}(t)$ decreases from its initial value $C_{22}(0) = 1$, then undershoots its asymptotic limit $\frac{1}{4} + \delta_4$, and approaches this limit by oscillating about it for a rather long time. On the other hand, spins of different sites are initially uncorrelated at infinite temperature, $C_{12}(0) = C_{24}(0) = 0$. At later times, these functions both overshoot their respective asymptotic limits $\frac{1}{4} - \delta_4$ and $\frac{1}{4} + \delta_4$, and then oscillate about them. The oscillations of $C_{12}(t)$ decay so rapidly that they are barely discernible in this figure. On the other hand the oscillations of $C_{24}(t)$ are of the same amplitude and persist as long as do those of $C_{22}(t)$, and are likewise easily seen in this figure. In addition, after $C_{22}(t)$ and $C_{24}(t)$ first become equal to each other, they braid about each other in their approaches to the same asymptotic limit.

In order to see more clearly how this occurs, we have found analytic expressions for the leading behaviors of the correlation functions for long times, $t \gg \tau$. We first consider $C_{12}(t)$. In this case, besides the constant I_0 , we only need to evaluate $I_1(t)$. To do so, we integrate both terms in Eq. (56) by parts, treating $\cos(st^*)$ as the variable to be integrated, and $f_1(s)$ and $g_1(s)$ as the variables to be differentiated. From the results in the Appendix, it is seen that $f_1(s)$ and $g_1(s)$ as well as their first three derivatives are continuous at $s = 2$. In addition, since the relevant integration endpoint values and derivatives at $s = 0$ and $s = 4$ also make no contribution through third order in the repeated integrations by parts, the leading contribution to the asymptotic behavior arise from the non-vanishing $f_1'''(0)$ and $g_1'''(4)$. The final result for the leading behavior is given by

$$\lim_{\substack{T \rightarrow \infty \\ t \gg \tau}} C_{12}(t) \rightarrow \frac{1}{4} - \delta_4 + \frac{1}{4t^{*4}} \left[\frac{3}{4} - \cos(4t^*) \right]. \quad (59)$$

On the other hand, $C_{22}(t)$ and $C_{24}(t)$ at infinite temperature also depend upon $I_2(t)$ and $I_3(t)$. Again, we integrate by parts in a similar fashion, treating $f_2(s)$, $f_3(s)$, $g_3(s)$, and $h_3(s)$ as the variables to be differentiated. The leading non-vanishing contributions to $C_{22}(t)$ and $C_{24}(t)$ from these integrations by parts are both of second order. For $I_2(t)$, the leading non-vanishing contribution comes from the non-vanishing $f_2'(0)$ and $f_2'(2)$, the latter of which is a non-trivial number. For $I_3(t)$, the leading non-vanishing contribution arises from $f_3'(0)$, $f_3'(2)$ and $g_3'(2)$. Although both $f_3(s)$ and $g_3(s)$ have non-trivial values and derivatives at their matching point $s = 2$, the difference between their derivatives is a trivial, but non-vanishing value. In addition, the functions $f_3(s)$ and $g_3(s)$ both have non-trivial values and derivatives at their

matching point $s = 4$, but these values and derivatives are equal, and thus their contribution in second order to the integration by parts vanishes. We thus obtain the long-time behaviors at infinite temperature,

$$\lim_{\substack{T \rightarrow \infty \\ t \gg \tau}} C_{22}(t) \rightarrow \frac{1}{4} + \delta_4 + \frac{1}{60t^{*2}} [5 - (29 + 8 \ln 2) \cos(2t^*)], \quad (60)$$

and

$$\lim_{\substack{T \rightarrow \infty \\ t \gg \tau}} C_{24}(t) \rightarrow \frac{1}{4} + \delta_4 - \frac{1}{60t^{*2}} [5 - (29 + 8 \ln 2) \cos(2t^*)]. \quad (61)$$

We note that $C_{12}(t)$ decays much more rapidly ($\propto 1/t^{*4}$) to its constant long-time limit than do either $C_{22}(t)$ or $C_{24}(t)$ ($\propto 1/t^{*2}$). The long-time braiding of these functions about each other arises from the opposite signs of their oscillatory terms. Furthermore, at long times, $C_{12}(t)$ oscillates with twice the frequency of the long-time oscillations of $C_{22}(t)$ and $C_{24}(t)$.

C. Results for finite temperatures

At finite T , we evaluate $I_0(\alpha)$ and $\langle S^2 \rangle(\alpha)$ numerically. For $|\alpha| < 1$, breaking each integral into 100 intervals is sufficient to obtain 0.1% accuracy. Note that this means there are 10^6 integration intervals overall. However, for low T ($|\alpha| > 1$), the number of intervals necessary to obtain that degree of accuracy increases. At $|\alpha| = 10$, one needs to break up each integration domain into 400 intervals, for instance. In Fig. 4, we have plotted the infinite-time limit of the spin-spin correlation functions $I_0(\alpha)$ and $\langle S^2 \rangle / 8 - I_0(\alpha)$ for both the ferromagnetic (FM) and antiferromagnetic (AFM) cases. As $\alpha \rightarrow 0$, one obtains the analytic limits given by Eqs. (53) and (54). However, in the low T limit $|\alpha| \rightarrow \infty$, both I_0 and $\langle S^2 \rangle / 8 - I_0 \rightarrow 0(1)$ for the AFM (FM) case, respectively. This just tells us that at $T = 0$, all of the spins are aligned in the FM case, and in the AFM case, their sum is 0. We note that for $|\alpha| \ll 1$, $I_0(\alpha)$ obeys the inversion symmetry, equivalent to $\partial I_0 / \partial \alpha \Big|_{\alpha=0}$ exists. We note that for the AFM case, $\lim_{t \rightarrow \infty} C_{12}(t)$ is negative for $\alpha < -0.71$. This just reflects the fact that for the antiferromagnetic ring, the spins on neighboring sites are anticorrelated at long times and for temperatures that are not too large.

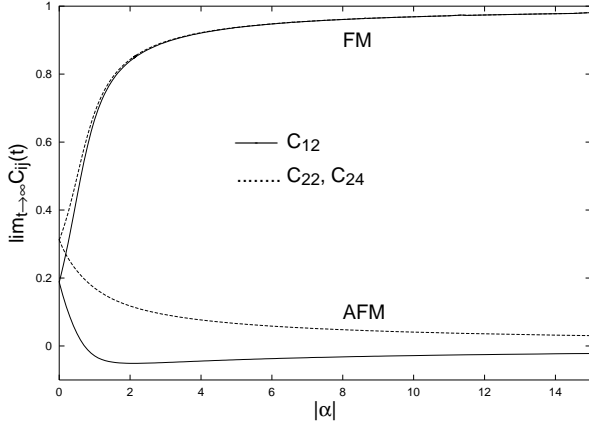


FIG. 4. Plot of $I_0(\alpha) = \lim_{t \rightarrow \infty} C_{22}(t) = \lim_{t \rightarrow \infty} C_{24}(t)$ and $\langle S^2 \rangle / 8 - I_0(\alpha) = \lim_{t \rightarrow \infty} C_{12}(t)$, as a function of $|\alpha|$, for the FM ($\alpha > 0$) and AFM ($\alpha < 0$) cases.

At finite T we also may evaluate the $I_i(t)$ numerically from the triple integral forms, Eqs. (44) - (46). As for I_0 , we break each of the three integrals into N intervals. At the lowest T values considered ($\alpha = -20$), it is necessary to take $N \geq 1000$ to achieve sufficient accuracy. In Figs. 5-7, we have plotted the $C_{ij}(t)$ for the FM case with $\alpha = 0.5, 2$, and 10 , and compared with the analytic results for $\alpha = 0$. In each of these figures, $C_{12}(t)$ decays to the equilibrium value $\langle S^2 \rangle / 8 - I_0(\alpha)$ more rapidly than $C_{22}(t)$ and $C_{24}(t)$ decay to their mutual equilibrium value $I_0(\alpha)$, while oscillating for a few periods about the latter. As T decreases, all of the $C_{ij}(0)$ increase monotonically, approaching unity as $T \rightarrow 0$. In addition, the oscillations persist to much longer times. Also, as seen in Figs. 5 and 8, as T decreases, $C_{12}(t)$ oscillates for an increasing amount of time, and $C_{22}(t)$ and $C_{24}(t)$ oscillate about it for an even longer period of time.

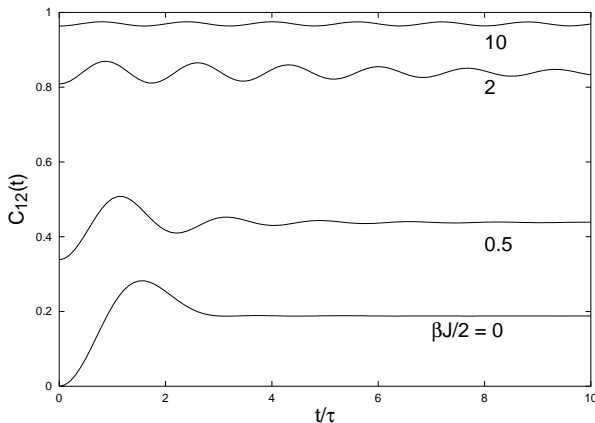


FIG. 5. Plots of $C_{12}(t)$ versus t/τ for the $\alpha = \beta J/2$ FM cases $0, 0.5, 2$, and 10 , as indicated.

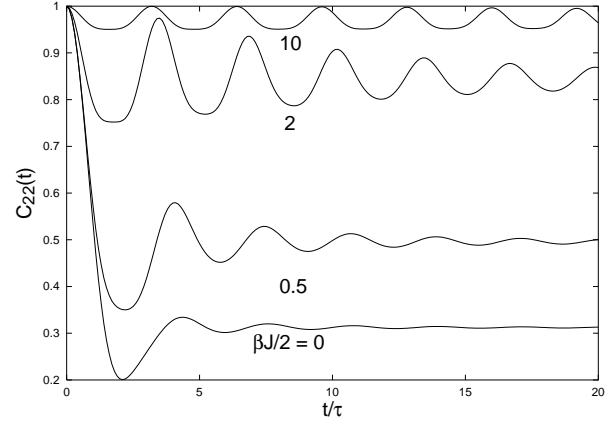


FIG. 6. Plots of $C_{22}(t)$ versus t/τ for the $\alpha = \beta J/2$ FM cases $0, 0.5, 2$, and 10 , as indicated.

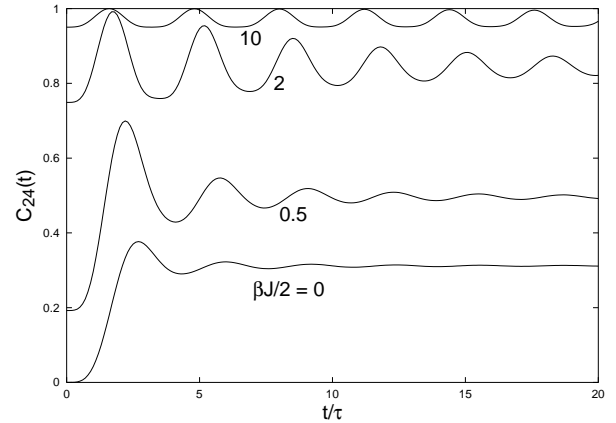


FIG. 7. Plots of $C_{24}(t)$ versus t/τ for the $\alpha = \beta J/2$ FM cases $0, 0.5, 2$, and 10 , as indicated.

At lower T , the amplitudes of the oscillations eventually reach a maximum, so that the oscillations in $C_{12}(t)$ for $\alpha = 0.5, 2, 10$ are distinctly noticeable. As $T \rightarrow 0$, the lifetimes of the oscillations appear to diverge, but their amplitudes become vanishingly small. At $\alpha = 10$, we have shown the behaviors of $C_{12}(t)$ (solid), $C_{22}(t)$ (dashed), and $C_{24}(t)$ (dotted) together in Fig. 8 for the extended time domain $0 \leq t/\tau \leq 30$. Throughout this domain, the decay of the oscillations in all three correlation functions is small but discernible. However, careful inspection of the oscillating waveforms reveals that $C_{12}(t)$ oscillates with twice the frequency of the other two, continuing the pattern that we have already seen for infinite temperature. Note that $C_{12}(t)$ appears to oscillate nearly as a simple cosine function, but $C_{22}(t)$ and $C_{24}(t)$ have a more complicated oscillatory behavior, with a fundamental frequency that is one-half that of $C_{12}(t)$, and they are almost completely out of phase with respect to one another.

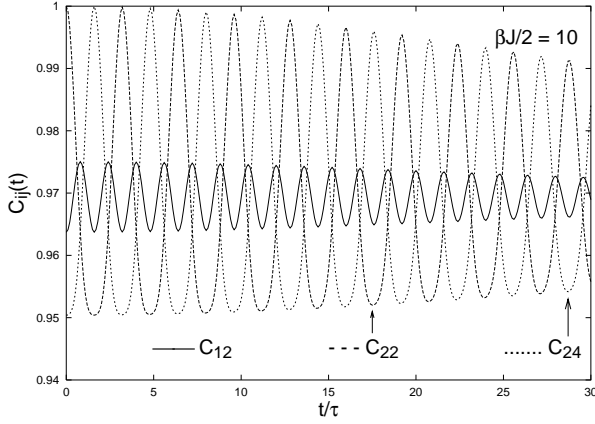


FIG. 8. Plot of $C_{12}(t)$ (solid), $C_{24}(t)$ (dotted), and $C_{22}(t)$ (dashed) versus t/τ for the low temperature FM case $\alpha = \beta J/2 = 10$. Note that $C_{22}(0) = 1$ and $C_{24}(0) \approx 0.95$.

The corresponding results for the AMF case are shown in Figs. 9-11, for which $\alpha = -0.5, -2$, and -20 , respectively. The last of these, $\alpha = -20$, took weeks of computational time to obtain sufficient accuracy. In these cases, we presented the $C_{12}(t)$, $C_{22}(t)$, and $C_{24}(t)$ data as solid, dashed, and dotted curves, respectively. We note that as the temperature is lowered, $C_{12}(0)$ decreases towards the value -1 , which would correspond to perfect AFM behavior. However, $C_{12}(t)$ then increases with t , reaches a maximum, and then decreases to the asymptotic, infinite time limit. In addition, as T is lowered, $C_{24}(0)$ increases towards $+1$, approaching $C_{22}(0)$. Then, at some time t_1 , $C_{22}(t_1)$ first equals $C_{24}(t_1)$, and thereafter, the two functions are braided about each other. The braiding oscillations decrease in amplitude as T is decreased, so that the overall $C_{ij}(t)$ all approach non-oscillatory uniform curves as $T \rightarrow 0$.

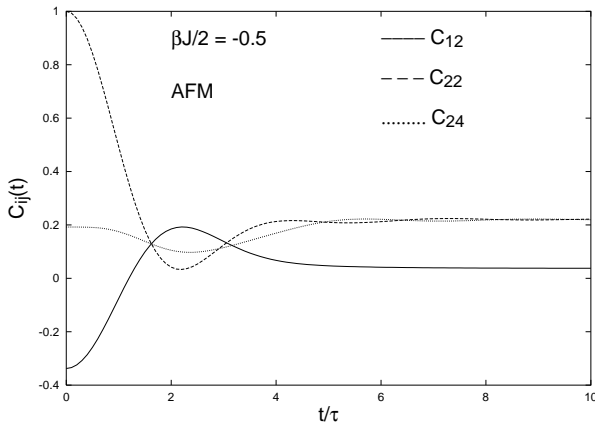


FIG. 9. Plot of $C_{12}(t)$ (solid), $C_{24}(t)$ (dotted), and $C_{22}(t)$ (dashed) versus t/τ for the AFM case $\alpha = -0.5$.

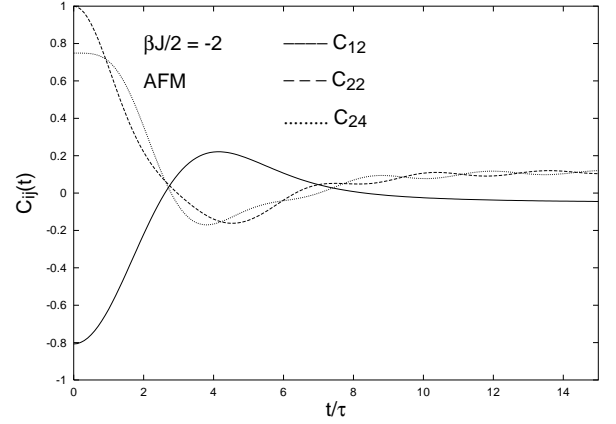


FIG. 10. Plot of $C_{12}(t)$ (solid), $C_{24}(t)$ (dotted), and $C_{22}(t)$ (dashed) versus t/τ for the AFM case $\alpha = -2$.

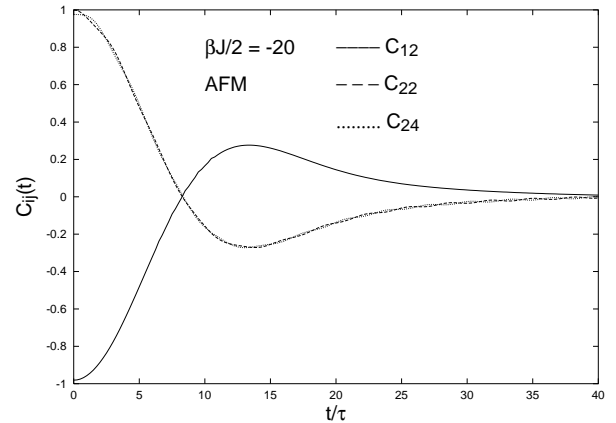


FIG. 11. Plot of $C_{12}(t)$ (solid), $C_{24}(t)$ (dotted), and $C_{22}(t)$ (dashed) versus t/τ for the very low temperature AFM case $\alpha = -20$.

From numerical simulation studies of more complicated mesoscopic classical systems, it has been suggested that the low temperature AFM autocorrelation function should scale, approaching uniform functions of $tT^{1/2}$. [24] To investigate whether such a scenario holds for this exactly solved four-spin system, we first plotted the AFM autocorrelation function at the low T values we considered. This is shown in Fig. 12. Although there are oscillations that persist to increasing times as T is lowered, the overall shape of the curves does not change its shape qualitatively, suggesting that $C_{22}(t)$ might indeed scale as a single function of $tT^{1/2}$ as $T \rightarrow 0$. In fact, this behavior has been established by analytical means for the simpler cases of the classical dimer, equilateral triangle, and regular tetrahedron. [21,23]

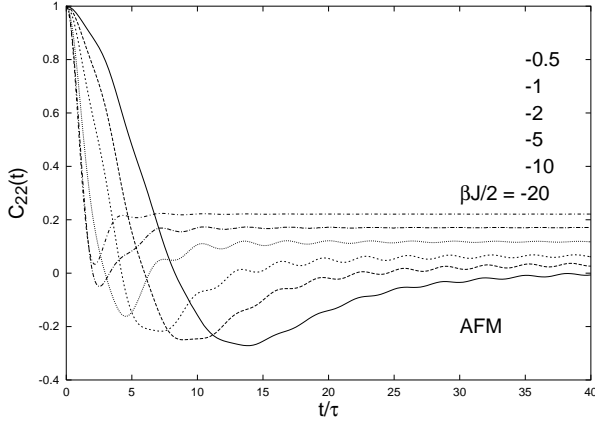


FIG. 12. Plot of $C_{22}(t)$ for the $\alpha = \beta J/2$ AFM cases -0.5 , -1 , -2 , -5 , -10 , and -20 , correspondingly from top to bottom at large t/τ , as indicated.

In Fig. 13, we therefore plotted $C_{22}(t)$ versus $t/[\tau|\beta J/2|^{1/2}]$, which is proportional to $tT^{1/2}$, to check this notion quantitatively. Indeed, the curves do scale, except for the braiding oscillations, which are decreasing in magnitude as T decreases. Thus, curves for the lowest two temperatures, $\alpha = -10$ and $\alpha = -20$, would nearly fall on top of each other if the oscillations were not present. Similar low temperature scaling behavior of $C_{24}(t)$ is shown in Fig. 14, which also includes the braiding oscillations. $C_{12}(t)$ exhibits a clearer example of the scaling, as shown in Fig. 15, since it does not contain any braiding oscillations. The major deviation from scaling occurs at very short times, although the differences between the curves at $\alpha = -10$ and $\alpha = -20$ are not so large there. Since $C_{12}(0) = -1$ in the zero temperature limit, this deviation from scaling probably arises from the fact that the $T = 0$ limit has not yet been reached for such short times.

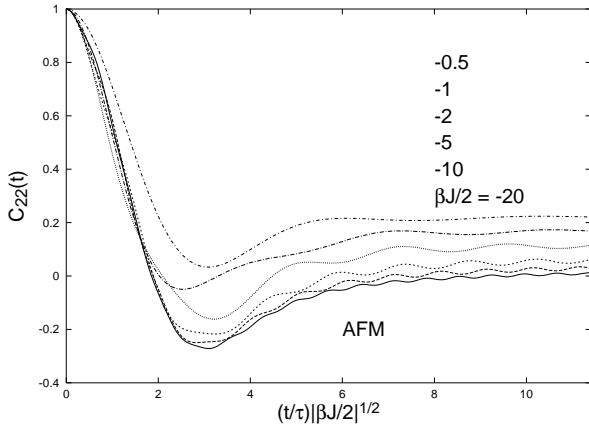


FIG. 13. Plot of $C_{22}(t)$ as a function of the scaled time $(t/\tau)|\beta J/2|^{1/2}$, for the $\alpha = \beta J/2$ AFM cases -0.5 , -1 , -2 , -5 , -10 , and -20 , correspondingly from top to bottom at large t/τ , as indicated.

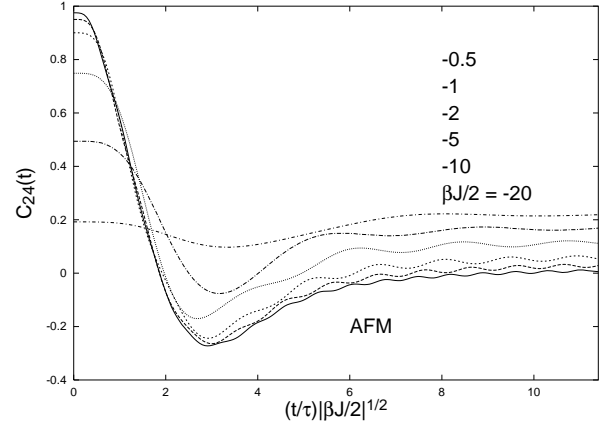


FIG. 14. Plot of $C_{24}(t)$ as a function of the scaled time $(t/\tau)|\beta J/2|^{1/2}$, for the $\alpha = \beta J/2$ AFM cases -0.5 , -1 , -2 , -5 , -10 , and -20 , correspondingly from top to bottom at large t/τ , as indicated.

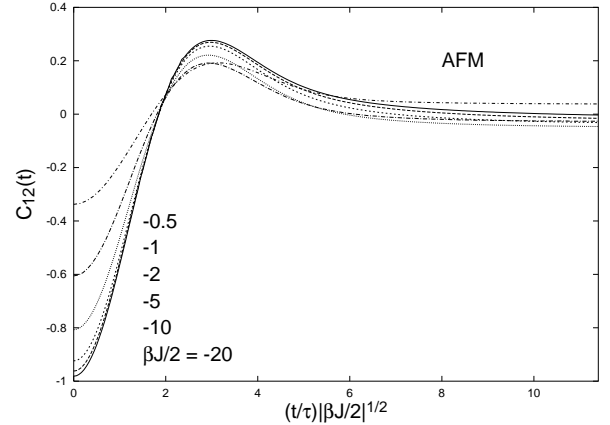


FIG. 15. Plot of $C_{12}(t)$ as a function of the scaled time $(t/\tau)|\beta J/2|^{1/2}$, for the $\alpha = \beta J/2$ AFM cases -0.5 , -1 , -2 , -5 , -10 , and -20 , correspondingly from top to bottom at small t/τ , as indicated.

At higher temperatures, the scaling property gradually breaks down. This is clearly seen for $\alpha = -0.5$ in Figs. 14 at 15, for which the short-time values of $C_{24}(t)$ and $C_{12}(t)$ deviate greatly from the values $(1$ and $-1)$ obtained respectively in the low temperature limit $\alpha \rightarrow -\infty$. For $C_{12}(t)$, the deviations are also rather large at long times. However, for all three correlation functions, even at $\alpha = -0.5$, the positions of the dip for $C_{22}(t)$ and $C_{24}(t)$ and the peak for $C_{12}(t)$ still scale.

D. Fourier Transforms

We now evaluate the Fourier transforms $\tilde{I}_i(\omega)$ of the $I_i(t)$. Since $C_{22}(t)$ and $C_{24}(t)$ both approach the constant $I_0 \neq 0$ as $t \rightarrow \infty$, and $C_{12}(t)$ approaches $\langle S^2 \rangle / 8 - I_0 \neq 0$ in the same limit, the $I_0 \neq 0$ or $\langle S^2 \rangle / 8 - I_0 \neq 0$ present in

the respective $\mathcal{C}_{ij}(t)$ give rise to delta functions in terms of the angular frequency ω , in $\tilde{\mathcal{C}}_{ij}(\omega)$, equal to either $2\pi I_0\delta(\omega)$ or $2\pi(\langle s^2 \rangle/8 - I_0)\delta(\omega)$, which can be written down by inspection from Eq. (43). We shall therefore evaluate the Fourier transform of the deviations $\delta\mathcal{C}_{ij}(t) = \mathcal{C}_{ij}(t) - \lim_{t \rightarrow \infty} \mathcal{C}_{ij}(t)$,

$$\begin{aligned}\tilde{\mathcal{C}}_{ij}(\omega) &= \int_{-\infty}^{\infty} dt e^{-i\omega t} \mathcal{C}_{ij}(t) \\ &= 2\pi I_0\delta(\omega) + \delta\tilde{\mathcal{C}}_{ij}(\omega)\end{aligned}\quad (62)$$

for $(i, j) = (2, 2)$ and $(2, 4)$, and

$$\tilde{\mathcal{C}}_{12}(\omega) = 2\pi(\langle S^2 \rangle/8 - I_0)\delta(\omega) + \delta\tilde{\mathcal{C}}_{12}(\omega), \quad (63)$$

where

$$\delta\tilde{\mathcal{C}}_{ij}(\omega) = \int_{-\infty}^{\infty} dt e^{-i\omega t} \delta\mathcal{C}_{ij}(t). \quad (64)$$

Causality requires that $\delta\tilde{\mathcal{C}}_{ij}(-\omega) = \delta\tilde{\mathcal{C}}_{ij}(\omega)$. Thus, it suffices to evaluate the $\delta\tilde{\mathcal{C}}_{ij}(\omega)$ for $\omega \geq 0$. For simplicity, we first evaluate $\tilde{I}_2(\omega)$, and let $\tilde{\omega} = \omega\tau$. Since the only time-dependence within the expression for $I_2(t)$ appears in the factor $\cos(yt/\tau)$, Fourier transformation replaces this factor with $[\delta(\omega - y/\tau) + \delta(\omega + y/\tau)]/2$, which can be written as $(\tau/2)[\delta(y - \tilde{\omega}) + \delta(y + \tilde{\omega})]$. The second δ -function does not contribute to the Fourier transform for $\omega > 0$, so we obtain for $\omega \geq 0$,

$$\begin{aligned}\tilde{I}_2(\omega) &= \frac{\pi\tau\Theta(2 - \tilde{\omega})(1 - \tilde{\omega}^2/4)}{8\tilde{\omega}\bar{Z}} \int_0^2 dx \int_{-1}^1 dz e^{2\alpha\tilde{\omega}xz} \times \\ &\quad \times \left(x^2 + \tilde{\omega}^2 - 2xz\tilde{\omega} - \frac{(x^2 - \tilde{\omega}^2)^2}{x^2 + \tilde{\omega}^2 + 2xz\tilde{\omega}} \right),\end{aligned}\quad (65)$$

where $\Theta(x)$ is the Heaviside step function, and we have made the change of variables $s^2 \rightarrow x^2 + \tilde{\omega}^2 + 2xz\tilde{\omega}$ for ease of computation.

We now evaluate $\tilde{I}_1(\omega)$. As in the expression for $\tilde{I}_2(\omega)$, Fourier transformation of the factor $\cos(st/\tau)$ replaces it with $(\tau/2)[\delta(s - \tilde{\omega}) + \delta(s + \tilde{\omega})]$, and the second term does not contribute to the integrals for $\omega > 0$. However, since $0 \leq s \leq 4$, there are now two regions of integration over the variables x and y . For $2 \leq \tilde{\omega} \leq 4$, the only region of integration is the interior of the isosceles triangle with sides obeying $x = 2$, $y = 2$, and $x + y = \tilde{\omega}$, and corners at their intersections. For $0 \leq \tilde{\omega} \leq 2$, the region of integration is the interior of the pentagon with sides obeying $y = 2$, $x = 2$, $y - x = -\tilde{\omega}$, $y + x = \tilde{\omega}$, and $y = x + \tilde{\omega}$. This interior region is symmetric about the line $y = x$, and can be broken up into two regions of integration. The first region is the interior of a rectangle rotated 45° about the axis normal to the xy plane, with sides obeying $y = x \pm \tilde{\omega}$ and $x + y = 2 \pm (2 - \tilde{\omega})$. The second region is the interior of the isosceles triangle with sides obeying $y = 2$, $x = 2$, and $y = -x + 4 - \tilde{\omega}$.

In the triangular integration regions, we maintain the integration variables x and y , keeping account of the integration limits. However, in the rectangular integration region, it is convenient to perform a rotation of the axes by 45° , letting $r = x - y$, $s = x + y$, and incorporating the Jacobian, which replaces the differential integration area $dx dy$ with $dr ds/2$. We thus have

$$\begin{aligned}\tilde{I}_1(\omega) &= \frac{\pi\tau\Theta(\tilde{\omega} - 2)\Theta(4 - \tilde{\omega})}{16\tilde{\omega}\bar{Z}} \int_{\tilde{\omega}-2}^2 dx \int_{\tilde{\omega}-x}^2 dy \times \\ &\quad \times e^{\alpha(\tilde{\omega}^2 - x^2 - y^2)} [_{-\tilde{\omega}^4} \\ &\quad + 2\tilde{\omega}^2(x^2 + y^2) - (x^2 - y^2)^2] \\ &\quad + \frac{\pi\tau\Theta(2 - \tilde{\omega})}{16\tilde{\omega}\bar{Z}} \int_{2-\tilde{\omega}}^2 dx \int_{4-x-\tilde{\omega}}^2 dy \times \\ &\quad \times e^{\alpha(\tilde{\omega}^2 - x^2 - y^2)} [_{-\tilde{\omega}^4} \\ &\quad + 2\tilde{\omega}^2(x^2 + y^2) - (x^2 - y^2)^2] \\ &\quad + \frac{\pi\tau\Theta(2 - \tilde{\omega})}{16\tilde{\omega}\bar{Z}} \int_0^{\tilde{\omega}} dr \int_{\tilde{\omega}}^{4-\tilde{\omega}} ds e^{\alpha[\tilde{\omega}^2 - (r^2 + s^2)/2]} \times \\ &\quad \times [_{-\tilde{\omega}^4 + \tilde{\omega}^2(r^2 + s^2) - r^2 s^2}].\end{aligned}\quad (66)$$

Last, but by no means least, we evaluate $\tilde{I}_3(\omega)$. This is easiest to do if we first use the trigonometric relations to rewrite Eq. (46) in terms of $\cos[(y + s)t/\tau]$ and $\cos[(y - s)t/\tau]$. Then, after Fourier transformation, we obtain,

$$\begin{aligned}\tilde{I}_3(\omega) &= \frac{\pi\tau}{16\bar{Z}} \int_0^2 dx \int_0^2 dy \frac{(1 - y^2/4)}{y^2} \int_{|x-y|}^{x+y} \frac{ds}{s} \times \\ &\quad \times e^{\alpha(s^2 - x^2 - y^2)} \left([(y + s)^2 - x^2]^2 [\delta(\tilde{\omega} + y - s) \right. \\ &\quad \quad \quad \left. + \delta(\tilde{\omega} - y + s)] \right. \\ &\quad \left. + [(y - s)^2 - x^2]^2 [\delta(\tilde{\omega} + y + s) \right. \\ &\quad \quad \quad \left. + \delta(\tilde{\omega} - y - s)] \right).\end{aligned}\quad (67)$$

For $\omega \geq 0$, the term containing $\delta(\tilde{\omega} + y + s)$ vanishes, so we are left with three terms, which we examine separately. We denote them \tilde{I}_{3n} , where $n = 1, 2, 3$, corresponding to the order in which the remaining δ -functions appear in Eq. (67). The first integral, \tilde{I}_{31} , is subject to the constraints $|x - y| \leq \tilde{\omega} + y \leq x + y$. The second ($\tilde{\omega} + y \leq x + y$) of these two constraints implies $\tilde{\omega} \leq x$, which also implies $0 \leq \tilde{\omega} \leq 2$. If $y < x$, the first constraint implies $y \geq (x - \tilde{\omega})/2$. On the other hand, if $x > y$, there is no additional constraint on the integration region, other than $x \geq \tilde{\omega}$. Thus, the combined integration region of this integral is the interior of an irregular quadrangle with sides obeying $x = \tilde{\omega}$, $y = 2$, $x = 2$, and $y = (x - \tilde{\omega})/2$. Hence, we may now write $\tilde{I}_{31}(\omega)$ by inspection,

$$\begin{aligned}\tilde{I}_{31}(\omega) &= \frac{\pi\tau\Theta(2 - \tilde{\omega})}{16\bar{Z}} \int_{\tilde{\omega}}^2 dx \int_{(x-\tilde{\omega})/2}^2 dy \frac{(1 - y^2/4)}{y^2(\tilde{\omega} + y)} \times \\ &\quad \times e^{\alpha(\tilde{\omega}^2 + 2\tilde{\omega}y - x^2)} [(2y + \tilde{\omega})^2 - x^2]^2.\end{aligned}\quad (68)$$

The integration regime of the second integral, $\tilde{I}_{32}(\omega)$ is subject to the constraints $|x - y| \leq y - \tilde{\omega} \leq x + y$.

The second ‘‘constraint’’ makes no restrictions for $\tilde{\omega} \geq 0$. However, the first constraint can be rewritten as $\tilde{\omega} \leq y - |x - y|$, and since x and y are both between 0 and 2, this then implies $0 \leq \tilde{\omega} \leq 2$. For $x > y$, the first constraint further requires $y \geq (\tilde{\omega} + x)/2$. On the other hand, for $y > x$, the first constraint requires $x \geq \tilde{\omega}$. Thus, the integration region is the interior of the irregular quadrangle with sides obeying $x = \tilde{\omega}$, $y = 2$, $x = 2$, and $y = (\tilde{\omega} + x)/2$. We therefore write

$$\tilde{I}_{32}(\omega) = \frac{\pi\tau\Theta(2-\tilde{\omega})}{16\bar{Z}} \int_{\tilde{\omega}}^2 dx \int_{(\tilde{\omega}+x)/2}^2 dy \frac{(1-y^2/4)}{y^2(y-\tilde{\omega})} \times e^{\alpha(\tilde{\omega}^2-2y\tilde{\omega}-x^2)} [(2y-\tilde{\omega})^2-x^2]^2. \quad (69)$$

Finally, the integration region of $\tilde{I}_{33}(\omega)$ is subject to the constraints $|x - y| \leq \tilde{\omega} - y \leq x + y$. The second constraint implies that $\tilde{\omega}$ can be as large as 6, and also that $y \geq (\tilde{\omega} - x)/2$. For $x > y$, the first constraint implies $x \leq \tilde{\omega}$, whereas for $y > x$, it implies $y \leq (\tilde{\omega} + x)/2$. For $0 \leq \tilde{\omega} \leq 2$, these constraints restrict the integration region to the interior of the triangle with sides obeying $y = (\tilde{\omega} - x)/2$, $y = (\tilde{\omega} + x)/2$, and $x = \tilde{\omega}$. For $4 \leq \tilde{\omega} \leq 6$, the integration region is the interior of the triangle with sides obeying $y = 2$, $x = 2$, and $y = (\tilde{\omega} - x)/2$. In the intermediate regime $2 \leq \tilde{\omega} \leq 4$, the integration region is the interior of the irregular quadrangle with sides obeying $y = (\tilde{\omega} - x)/2$, $y = (\tilde{\omega} + x)/2$, $y = 2$, and $x = 2$. We break this integration region up into two parts. One of these parts is the interior of the isosceles triangle with sides obeying $y = (\tilde{\omega} - x)/2$, $y = (\tilde{\omega} + x)/2$, and $x = 4 - \tilde{\omega}$. The second region is the interior of the irregular quadrangle with sides obeying $x = 4 - \tilde{\omega}$, $y = 2$, $x = 2$, and $y = (\tilde{\omega} - x)/2$. Altogether, we write $\tilde{I}_{33}(\omega)$ as

$$\begin{aligned} \tilde{I}_{33}(\omega) &= \frac{\pi\tau\Theta(2-\tilde{\omega})}{16\bar{Z}} \int_0^{\tilde{\omega}} dx \int_{(\tilde{\omega}-x)/2}^{(\tilde{\omega}+x)/2} dy f(x, y, \tilde{\omega}) \\ &+ \frac{\pi\tau\Theta(\tilde{\omega}-2)\Theta(4-\tilde{\omega})}{16\bar{Z}} \times \\ &\times \left[\int_0^{4-\tilde{\omega}} dx \int_{(\tilde{\omega}-x)/2}^{(\tilde{\omega}+x)/2} dy \right. \\ &\quad \left. + \int_{4-\tilde{\omega}}^2 dx \int_{(\tilde{\omega}-x)/2}^2 dy \right] f(x, y, \tilde{\omega}) \\ &+ \frac{\pi\tau\Theta(\tilde{\omega}-4)\Theta(6-\tilde{\omega})}{16\bar{Z}} \times \\ &\times \int_{\tilde{\omega}-4}^2 dx \int_{(\tilde{\omega}-x)/2}^2 dy f(x, y, \tilde{\omega}), \quad (70) \end{aligned}$$

where

$$f(x, y, \tilde{\omega}) = \frac{(1-y^2/4)}{y^2(\tilde{\omega}-y)} e^{\alpha(\tilde{\omega}^2-2\tilde{\omega}y-x^2)} \times [(2y-\tilde{\omega})^2-x^2]^2. \quad (71)$$

In Figs. 16 - 20, we present our results for the $\delta\tilde{C}_{ij}(\omega)$, plotted as functions of $\omega\tau$. In the figure labels, we drop

the tildes for clarity. Note that these functions are rigorously zero for $\omega\tau > 6$, but they are so small for $\omega\tau > 4$ that they are indistinguishable from zero for $\omega\tau > 4.1$ in plots with $0 \leq \omega\tau \leq 6$. In each case, $\delta\tilde{C}_{12}(\omega)$ are the solid curves, $\delta\tilde{C}_{24}(\omega)$ are the dotted curves, and $\delta\tilde{C}_{22}(\omega)$ are the dashed curves. At infinite temperature, these are obtained from our exact formulae for the $f_i(s)$, $g_i(s)$ and $h_3(s)$ listed in the Appendix by simply letting $s \rightarrow \omega\tau$, and multiplying the overall results by π . For example, $\delta\tilde{C}_{12}(\omega) = -\pi[f_1(\omega\tau) + g_1(\omega\tau)]$. The exact expressions for the three $\delta\tilde{C}_{ij}(\omega)$ are plotted in Fig. 16. As a check on our computations, we also obtained these results by numerically evaluating the $\delta C_{ij}(t)$ from the double integrals in the infinite temperature limit, and the results were found to agree to within three significant figures.

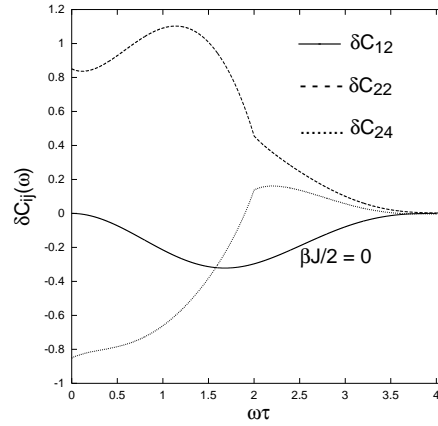


FIG. 16. Plots of the exact Fourier transforms $\delta\tilde{C}_{12}(\omega)$ (solid), $\delta\tilde{C}_{22}(\omega)$ (dashed), and $\delta\tilde{C}_{24}(\omega)$ (dotted) of $C_{ij}(t) - \lim_{t \rightarrow \infty} C_{ij}(t)$, as functions of $\omega\tau$, in the infinite temperature limit $\alpha = 0$.

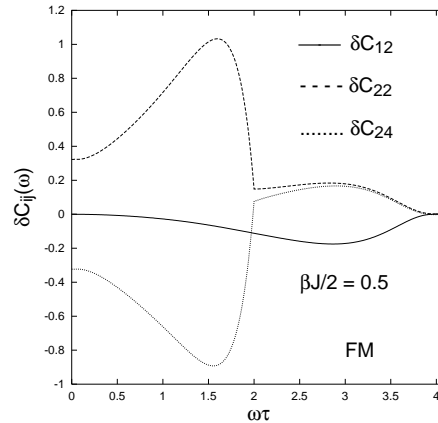


FIG. 17. Plots of the Fourier transforms $\delta\tilde{C}_{12}(\omega)$ (solid), $\delta\tilde{C}_{22}(\omega)$ (dashed), and $\delta\tilde{C}_{24}(\omega)$ (dotted) of $C_{ij}(t) - \lim_{t \rightarrow \infty} C_{ij}(t)$, as functions of $\omega\tau$, for the FM case $\alpha = 0.5$.

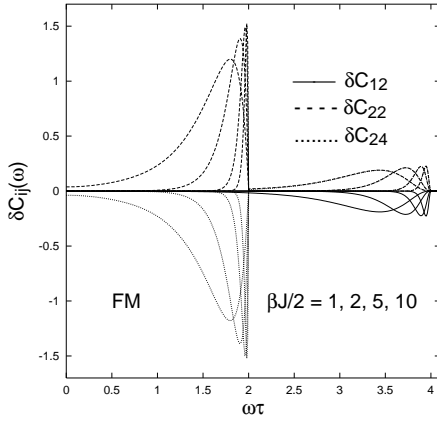


FIG. 18. Plots of the Fourier transforms $\delta\tilde{C}_{12}(\omega)$ (solid), $\delta\tilde{C}_{22}(\omega)$ (dashed), and $\delta\tilde{C}_{24}(\omega)$ (dotted) of $C_{ij}(t) - \lim_{t \rightarrow \infty} C_{ij}(t)$, as functions of $\omega\tau$, for the FM cases $\alpha = 1, 2, 5$, and 10 . The peaks developing successively near $\omega\tau = 2, 4$ with decreasing T are magnons.

In this and in subsequent figures, we also checked the accuracy of our analytic formulae by the zero-time sum rule, the $\int_0^\infty \delta\tilde{C}_{ij}(\omega) d\omega/\pi = \delta C_{ij}(0)$. It is seen that the functions all are continuous, and approach zero at large ω . $\delta\tilde{C}_{12}(\omega) \leq 0$, and $\delta\tilde{C}_{22}(\omega) \geq 0$, but $\delta\tilde{C}_{24}(\omega)$ has regions of both signs. In Figs. 17 and 18, we present the data for the FM case, with $\alpha = 0.5$ in Fig. 17, and $\alpha = 1, 2, 5$, and 10 in Fig. 18. As the temperature is lowered, the peak in $\delta\tilde{C}_{22}(\omega)$ moves to higher ω values. Moreover, $\delta\tilde{C}_{22}(\omega)$ and $\delta\tilde{C}_{24}(\omega)$ approach each other in the region $2 \leq \omega\tau \leq 4$, but approach the opposite of each other in the regime $0 \leq \omega\tau \leq 2$. Thus, in the regime $2 \leq \omega\tau \leq 4$ of Fig. 18, these dashed and dotted curves combine to give a curve that appears to be dash-dotted. In addition, as the temperature is lowered, the curves all develop into sharp peaks at $\omega\tau \approx 2$ and 4 , which are asymmetric, dropping rapidly to zero at $\omega\tau = 2$ and 4 , but having longer tails at lower $\omega\tau$ values. More precisely, $\delta\tilde{C}_{12}(\omega)$ becomes a single peak at $\omega\tau \approx 4$, whereas the other two, $\delta\tilde{C}_{22}(\omega)$ and $\delta\tilde{C}_{24}(\omega)$ have identical peaks at $\omega\tau \approx 4$, which are opposite to that of $\delta\tilde{C}_{12}(\omega)$. But, they also have larger and sharper peaks at $\omega\tau \approx 2$, which are opposite in sign to each other. These peaks at $\omega\tau \approx 2, 4$ arise from magnons. Hence, Fig. 18 provides a simple explanation of the detail of $C_{ij}(t)$ for $\alpha = 10$ shown in Fig. 8.

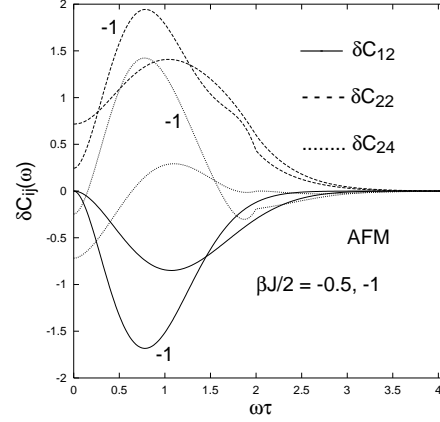


FIG. 19. Plots of the Fourier transforms $\delta\tilde{C}_{12}(\omega)$ (solid), $\delta\tilde{C}_{22}(\omega)$ (dashed), and $\delta\tilde{C}_{24}(\omega)$ (dotted) of $C_{ij}(t) - \lim_{t \rightarrow \infty} C_{ij}(t)$, as functions of $\omega\tau$, for the AFM cases $\alpha = -0.5$ and -1 . The bumps developing for $\alpha = -1$ at $\omega\tau \approx 2$ are magnons.

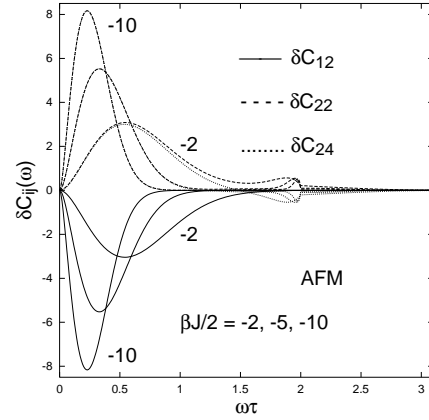


FIG. 20. Plots of the Fourier transforms $\delta\tilde{C}_{12}(\omega)$ (solid), $\delta\tilde{C}_{22}(\omega)$ (dashed), and $\delta\tilde{C}_{24}(\omega)$ (dotted) of $C_{ij}(t) - \lim_{t \rightarrow \infty} C_{ij}(t)$, as functions of $\omega\tau$, for the AFM cases $\alpha = -2, -5$, and -10 . The peaks for $\omega\tau \approx 2$ that successively sharpen with decreasing T are magnons.

Curves for the AFM case are shown in Fig. 19 and 20. In Fig. 19, we display the results for $\alpha = -0.5$ and -1 together, and in Fig. 20, the results for $\alpha = -2, -5$, and -10 are shown. As the temperature is lowered, the peak in $\delta\tilde{C}_{22}(\omega)$ moves to lower frequency, resulting in the slowing down seen in the real time curves. It develops into two peaks, a large one at low $\omega\tau$, and a small one at $\omega\tau \approx 2$, which is an antiferromagnetic magnon. Note that the magnon width sharpens as T is lowered. Surprisingly, $\delta\tilde{C}_{24}(\omega)$ changes dramatically, mostly changing sign near $\omega\tau \approx 2$, but the small ω behavior increases to join the small ω behavior of $\delta\tilde{C}_{22}(\omega)$, and the opposite of it in the region $\omega\tau \approx 2$. These peaks at $\omega\tau \approx 2$ arise from antiferromagnetic magnons. In addition, $\delta\tilde{C}_{12}(\omega)$ stays negative, and develops into a negative peak at low

ω which is opposite to that of $\delta\tilde{C}_{22}(\omega)$ and $\delta\tilde{C}_{24}(\omega)$.

Finally, in order to elucidate the nature of the slowing down as T is lowered, in Fig. 21 we plotted our AFM results for $\alpha = -0.5, -1, -2, -5, \text{ and } -10$ together, as a function of the scaled frequency $\omega\tau|\beta J/2|^{1/2}$. We note that the position of the low frequency peak does indeed scale, but since the magnon appears at a fixed frequency, it does not scale. The magnon is distinctly visible for $\alpha = -2, -5, \text{ and } -10$ in this figure, as noted by the arrows.

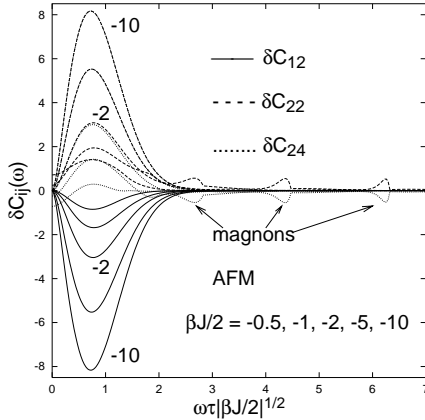


FIG. 21. Plots of the Fourier transforms $\delta\tilde{C}_{12}(\omega)$ (solid), $\delta\tilde{C}_{22}(\omega)$ (dashed), and $\delta\tilde{C}_{24}(\omega)$ (dotted) of $C_{ij}(t) - \lim_{t \rightarrow \infty} C_{ij}(t)$, as functions of the scaled frequency $\omega\tau|\beta J/2|^{1/2}$, for the AFM cases $\alpha = -0.5, -1, -2, -5, \text{ and } -10$. The magnon peaks for $\omega\tau \approx 2$ do not scale, and are marked with arrows.

IV. DISCUSSION AND CONCLUSIONS

In this paper we have presented the exact solution for the thermal equilibrium dynamics of four classical Heisenberg spins on a ring. For this system, there are three relevant time correlation functions, which are the auto- (C_{22}), near-neighbor (C_{12}), and the next-nearest-neighbor (C_{24}) correlation functions, respectively. Using our results, we wrote exact expressions for these three functions in terms of triple integrals. At infinite temperature, we reduced these triple integrals to single integrals. We also obtained analytic expressions for the long-time, infinite temperature behavior of the three correlation functions. We found that the near-neighbor correlation function $C_{12}(t)$ is strikingly different from the auto- and next-nearest-neighbor correlation functions $C_{22}(t)$ and $C_{24}(t)$. Not only does it approach a different finite value asymptotically, but it also oscillates with twice the frequency, and the oscillations decay in amplitude much more rapidly. Although the long-time asymptotic values of these functions vary with temperature, the near-neighbor correlation function similarly differs from the other two functions for all temperatures.

In addition, we were able to obtain the Fourier transforms of the deviations of the correlation functions from their infinite time asymptotic limits in terms of double integrals. At infinite temperature, exact analytic forms for these Fourier transforms were obtained. As the temperature is lowered, peaks in the Fourier transforms appear at $\omega\tau = 2$ for antiferromagnetic coupling, and at $\omega\tau = 2, 4$ for ferromagnetic coupling. These peaks sharpen up as the temperature is lowered. Although the origin of these peaks is purely classical, they correspond precisely to magnons, which are usually thought of as quantum mechanical in origin. Here the magnons arise from standing waves, such as those on a violin string. These standing waves arise from the periodicity of the ring, as a combination of traveling waves moving both clockwise and counterclockwise in direction. For the antiferromagnetic case, neighboring spins are opposite in direction at low temperatures, so that two full wavelengths fit into the ring. For the ferromagnetic case, one can have either two or four full wavelengths in the ring, the latter corresponding to every spin pointing in the same direction.

In the quantum mechanical analogue, the magnon energies are $E_n = 2J[1 - \cos(k_n a)]$, where $k_n = 2n\pi/L$ and $L = 4a$. We thus get $E_0 = 0$, $E_1 = 2J$, and $E_2 = 4J$. These latter two values correspond precisely to $\omega\tau = 2, 4$.

In addition, for antiferromagnetic coupling, a second, much larger peak in the Fourier transform functions appears at increasing lower frequency as the temperature is lowered. This second peak is found to scale with $\omega/T^{1/2}$, corresponding to the $tT^{1/2}$ scaling of the low temperature antiferromagnetic time correlation functions.

It is interesting to compare the long-time asymptotic results of the correlation functions at infinite temperature with the known results for other Heisenberg rings. For a dimer, with two Heisenberg spins interacting via Eq. (1) with $\mathbf{S}_3 = \mathbf{S}_1$, the infinite temperature limit of the auto- and near-neighbor correlation functions were given for all t , [25]

$$\lim_{T \rightarrow \infty} C_{11}(t) = \frac{1}{2} - \frac{1 + 2 \cos(2t^*)}{2t^{*2}} + \frac{3 \sin(3t^*)}{2t^{*3}} - \frac{3[1 - \cos(2t^*)]}{4t^{*4}} \quad (72)$$

$$= 1 - \lim_{T \rightarrow \infty} C_{12}(t), \quad (73)$$

$$(74)$$

where we have used the conservation law,

$$C_{11}(t) + C_{12}(t) = \langle S^2 \rangle / 2, \quad (75)$$

and $\lim_{T \rightarrow \infty} \langle S^2 \rangle / 2 = 1$ for the dimer.

For the case of three spins on a ring, it is not so trivial, but it is still much easier to evaluate the correlation functions at large times and infinite temperature than for the four-spin ring. The infinite temperature asymptotic limit result for the autocorrelation function $C_{11}(t)$

was quoted previously, [25] and its complete derivation for all temperatures was given. [23] In this case, reduction to quadrature is rather simple, and one obtains a result for the three-spin ring $\delta\mathcal{C}_{11}(t)$ analogous to Eq. (56). At infinite temperature, [23]

$$\lim_{T \rightarrow \infty} \delta\mathcal{C}_{11}(t) = \int_0^1 ds f_4(s) \cos(st^*) + \int_1^3 ds g_4(s) \cos(st^*), \quad (76)$$

where $f_4(s)$, $g_4(s)$, and their values and relevant derivatives at the integration endpoints are given in the Appendix. Thus, for the three-spin ring, the leading terms for long times were shown to be, [23]

$$\lim_{\substack{T \rightarrow \infty \\ t \gg \tau}} \mathcal{C}_{11}(t) = \frac{1}{3} + \delta_3 - \frac{[\sin(t^*) + \sin(3t^*)]}{t^{*3}}, \quad (77)$$

where

$$\delta_3 = \frac{9}{40} \ln 3 - \frac{1}{10} \approx 0.147188. \quad (78)$$

In analogy with Eq. (50), it is then easy to see that

$$2\mathcal{C}_{12}(t) + \mathcal{C}_{11}(t) = \langle S^2 \rangle / 3, \quad (79)$$

and hence that

$$\lim_{\substack{T \rightarrow \infty \\ t \gg \tau}} \mathcal{C}_{12}(t) = \frac{1}{3} - \frac{\delta_3}{2} + \frac{[\sin(t^*) + \sin(3t^*)]}{2t^{*3}}, \quad (80)$$

since $\lim_{T \rightarrow \infty} \langle S^2 \rangle / 3 = 1$ for the three-spin ring.

For $N \geq 3$ classical Heisenberg spins on a ring, it is straightforward to obtain the conservation equation for the correlation functions,

$$\mathcal{C}_{11}(t) + 2 \sum_{n=2}^{(N+1)/2} \mathcal{C}_{1n}(t) = \langle S^2 \rangle / N, \quad (81)$$

and

$$\mathcal{C}_{11}(t) + 2 \sum_{n=2}^{N/2} \mathcal{C}_{1n}(t) + \mathcal{C}_{1,(N+2)/2}(t) = \langle S^2 \rangle / N, \quad (82)$$

for N odd and even, respectively.

We note that for $1 \leq N \leq 4$ at infinite temperature, $\langle S^2 \rangle / N = 1$. More generally, at infinite temperature, the evaluation of $\langle S^2 \rangle$ for an N -spin ring maps onto that of the mean square displacement of a chain of length N during a random walk in three dimensions, and hence rigorously $\lim_{T \rightarrow \infty} \langle S^2 \rangle / N = 1 \forall N \geq 1$. We then note that the long-time behavior of $\mathcal{C}_{11}(t)$ at infinite temperature arises primarily from the discontinuities in the derivatives of the functions $f_i(s)$, $g_i(s)$, $h_i(s)$, etc. at the endpoints of the integration intervals. For $N = 2, 4$, the functions are finite and continuous over the integration regions, but

at least one of their first derivatives is discontinuous at one or more of the integration endpoints. In addition, for the particular odd-spin ring with $N = 3$, both the functions and their first derivatives are continuous at the integration endpoints, but the second derivatives are discontinuous at the endpoints. The mathematical forms of the functions $f_i(s)$, $g_i(s)$, $h_i(s)$, etc. and their various derivatives at the integration endpoints become increasingly complicated with increasing N for $N \leq 4$.

It would be interesting to find out whether this ‘‘pattern’’ of matching the functions and their derivatives at the integration endpoints might be maintained for much larger N values. Thus, at least two possible scenarios that might develop from attempting to generalize our results to much larger N values arise. Regardless of whether N is even or odd, $\mathcal{C}_{11}(t)$ might behave for $t^* \gg 1$ as

$$\mathcal{C}_{11}(t) \rightarrow \begin{cases} \frac{1}{N} + \delta_N + \sum_{n=0}^N a_n \cos(nt^*) / t^{*2}, \\ \frac{1}{N} + \delta_N + \sum_{n=1}^N b_n \sin(nt^*) / t^*, \end{cases} \quad (83)$$

which would occur if the functions were finite and continuous but with one or more discontinuous first derivatives, as for $N = 2, 4$, or if they were finite but discontinuous at one or more of the integration endpoints, respectively. Of course, behavior such as for $N = 3$ could also be obtained for higher N values, as well, as well as more complicated scenarios. We expect that $\lim_{N \rightarrow \infty} \delta_N = 0$, and that δ_N decreases to zero faster than $1/N$. We note that for $N = 2$, we have $\delta_2 = 0$.

Numerical simulation data for the $N = 4, 6, 8, 10, 50$ autocorrelation functions were presented for $0 \leq t^* \leq 10$ by Müller. [17] Those results show that the oscillations in $\mathcal{C}_{11}(t)$ for $N \geq 4$ are easily discernible out to $t^* = 10$. Hence, it appears unlikely that the autocorrelation functions would approach their asymptotic limits more rapidly than $1/t^{*2}$. The high accuracy of the numerical results is exemplified by the excellent agreement between the result for $N = 4$ and our own exact analytical results, [17] as shown in Fig. 3b.

The main difference between rings with even and odd numbers N of spins lies in the long-time behaviors of the two-spin time correlation functions. For both N even and odd, the conservation law requires at least one of the \mathcal{C}_{1n} for $n \neq 1$ to compensate for the leading long-time behavior of $\mathcal{C}_{11}(t)$. For odd N , we anticipate that all of the correlation functions will fall off with oscillatory corrections that have an amplitude of order $(t^*)^{-m}$ at large times, where m is likely to be a small natural number. We then raise the question for even N , as to which, if any, of the correlation functions approaches its asymptotic limit more rapidly than the autocorrelation function does for long times. Based upon the $N = 2, 4$ examples, the answer to this question might depend upon whether $N/2$ is even or odd.

Finally, we turn to the unresolved question, vigorously debated in the literature for over a decade, [17,18,19,20] of whether the large- N limit of the two-spin correlation functions for rings of classical Heisenberg spins, based on the dynamics of Eq. (7), will decay to zero with the leading behavior $t^{-1/2}$ for long times. This asymptotic behavior can easily be derived for an infinite linear chain of classical spins whose dynamics are governed by the following discretized version of a continuous spin hydrodynamics,

$$\frac{d\mathbf{S}_i}{dt} = \gamma(\mathbf{S}_{i+1} + \mathbf{S}_{i-1} - 2\mathbf{S}_i). \quad (84)$$

The parameter $\gamma = D/a^2$, where a is the lattice constant, and D is a spin diffusion coefficient. The final result for the vector component μ of the two-spin correlation function for a pair of spins n lattice sites apart coincides with the probability distribution for a one-dimensional continuous time random walk from the origin, [26]

$$\langle S_i^\mu(0)S_{i+n}^\mu(t) \rangle = \exp(-t^*)I_n(t^*), \quad (85)$$

where now $t^* = 2\gamma t$ and $I_n(z)$ is a modified Bessel function. For fixed n , the leading behavior for large t is indeed proportional to $(t^*)^{-1/2}$.

For the four-spin ring with diffusive dynamics, Eq. (84), one finds at infinite temperature,

$$\mathcal{C}_{22}(t) = [1 + \exp(-t^*)]^2/4, \quad (86)$$

$$\mathcal{C}_{24}(t) = [1 - \exp(-t^*)]^2/4, \quad (87)$$

and

$$\mathcal{C}_{12}(t) = [1 - \exp(-2t^*)]/4, \quad (88)$$

but

$$\langle \mathbf{S}_i^2(t) \rangle = [1 + \exp(-2t^*)]^2/4 \quad (89)$$

for $i = 1, \dots, 4$. Although the three correlation functions are different, satisfying the conservation law, Eq. (50), and $\mathcal{C}_{12}(t)$ correctly reaches its asymptotic limit faster than do either of the other two, they all go exponentially to the same asymptotic value $1/4$, and do not exhibit any oscillations. In addition, the rms value of each individual spin magnitude decays from its assumed initial value of unity to $1/2$.

Generalizing this treatment to a closed finite ring with N sites, as derived using Eq. (84), leads to the following results. The corresponding time correlation functions all approach the same non-zero limit $1/N$ for long times, with correction terms that rise or decay as $\exp(-\mu_N t^*)$, where $\mu_N = 1 - \cos(2\pi/N)$. In addition, each rms individual spin magnitude decays exponentially from its initial value of unity to $1/N^{1/2}$. These features are distinctly different from the exact results we have obtained for the four-spin ring, and others have obtained for the

dimer and three-spin ring, [25,23] based upon Heisenberg dynamics, Eq. (7). However, the diffusive approximation does suggest that for N divisible by 4, $\mathcal{C}_{1,1+N/4}(t)$ should approach its asymptotic limit faster than the other correlation functions, as occurs in the exact treatment for $N = 4$. It would be interesting to see if qualitatively similar features are obtained for higher N values using Heisenberg dynamics.

It is noteworthy that as long as t is sufficiently small compared to $N^2/(2\gamma)$, the numerical results of the treatment for the N -spin ring based upon Eq. (84) are virtually indistinguishable from the result, Eq. (85), for the infinite chain. This can be expected, since the rms distance achieved by the corresponding random walker remains small compared to the circumference of the ring, hence for all intents and purposes the behavior should be the same as that of an infinite linear chain.

Now our main point is that diffusive spin dynamics based upon Eq. (84), while conserving the components of the total spin vector, *does not* preserve the length of the individual spin vectors. However, this property, $|\mathbf{S}_i(t)| = 1$ for $i = 1, \dots, N$, is of course maintained at all times by Heisenberg dynamics, Eq. (7). That is, *the spin dynamics based upon Eq. (84) are fundamentally different in character from those based upon Eq. (7)*. Not surprisingly, the present exact results at infinite temperature, Eqs. (56) - (58), displayed in Fig. 3a, along with the analytic expansions for long times, Eqs. (59) - (61), of the two-spin correlation functions for $N = 4$ spins based upon Heisenberg dynamics, Eq. (7), differ both quantitatively and qualitatively from the results, Eqs. (86) - (89), that one obtains using diffusive dynamics from the four-spin version of Eq. (84). These fundamental differences only underscore the fact that the broader question, of whether the time correlation functions derived from the Heisenberg spin dynamics, Eq. (7), will show a $t^{-1/2}$ long-time approach to their asymptotic limits, as does Eq. (85), is acute and deserving of greater attention.

V. ACKNOWLEDGMENTS

The authors would like to thank T. Bandos, D. Mentrup, K. Scharnberg, J. Schnack, and C. Schröder for very useful discussions. One of us (RAK) would like to thank the Ames Laboratory and the Max-Planck-Institut für Physik komplexer Probleme for their hospitality. The Ames Laboratory is operated by Iowa State University under Contract No. W-7405-Eng-82.

VI. APPENDIX

Here we list the functions $f_i(s)$, $g_i(s)$, and $h_i(s)$ for the correlation functions at infinite temperature. We find,

$$f_1(s) = \frac{1}{144}s^2(s-2)^2(s+4) - \frac{s^3}{2880}(5s^2 + 48s - 150), \quad (90)$$

$$g_1(s) = \frac{(4-s)^3}{2880s}(5s^3 + 12s^2 - 6s - 8), \quad (91)$$

$$f_2(s) = \frac{(4-s^2)}{480s^2} \left[12s + 11s^3 + s^5 \ln\left(\frac{s^2}{4-s^2}\right) - (12 - 10s^2 + \frac{15}{4}s^4) \ln\left(\frac{2+s}{2-s}\right) \right], \quad (92)$$

$$f_3(s) = a_1(s) + a_2(s)(2-s) \ln 2 + \frac{s^3(40-s^2)}{480} \ln\left(\frac{s}{s+2}\right) + a_3(s)(2-s)^2 \ln(4-s^2), \quad (93)$$

where

$$a_1(s) = \frac{1}{115200} (61264 - 28800s + 19160s^2 - 4160s^3 + 45s^4 + 188s^5), \quad (94)$$

$$a_2(s) = -\frac{1}{1920s^2} (96 + 48s + 608s^2 + 304s^3 - 318s^4 - 23s^5 - 4s^6), \quad (95)$$

and

$$a_3(s) = \frac{1}{320s^2} (4 + 4s + 13s^2 + 12s^3), \quad (96)$$

$$g_3(s) = b_1(s) + b_2(s) \ln 2 + \frac{s^3(s^2 + 32)}{480} \ln s + b_3(s) \ln(s-2) + b_4(s) \ln(s+2), \quad (97)$$

where

$$b_1(s) = \frac{1}{230400s} (-17280 - 28496s + 60000s^2 + 21800s^3 - 5600s^4 - 1485s^5 + 188s^6), \quad (98)$$

$$b_2(s) = -\frac{(s+2)}{3840s^2} (-96 + 48s - 608s^2 + 304s^3 + 318s^4 - 23s^5 + 4s^6), \quad (99)$$

$$b_3(s) = -\frac{(s-2)^2}{3840s^2} (96 + 96s + 140s^2 + 116s^3 + s^4 + 4s^5), \quad (100)$$

and

$$b_4(s) = -\frac{1}{3840s^2} (s-2)(s+2)^4(6-9s+4s^2), \quad (101)$$

and finally,

$$h_3(s) = \frac{(s-2)}{3840} \left[s^3(23+4s) \ln\left(\frac{2(s-2)}{s+2}\right) \right.$$

$$\left. + 2(92 + 46s - 57s^2) \ln\left(\frac{s-2}{4}\right) - 10(8 + 4s - 3s^2) \ln\left(\frac{8}{s+2}\right) + \frac{48(s+2)}{s^2} \ln\left(\frac{(s-2)^2}{2(s+2)}\right) \right] + c_1(s), \quad (102)$$

where

$$c_1(s) = \frac{(s-6)}{230400s} (2880 + 16152s - 22668s^2 + 6242s^3 + 267s^4 - 188s^5). \quad (103)$$

For the three-spin ring,

$$f_4(s) = \frac{s^2(5-s^2)}{15} \quad (104)$$

and

$$g_4(s) = \frac{(s-3)^2}{120s} (-3 - 2s + 9s^2 + 4s^3). \quad (105)$$

To obtain the leading long-time behavior of the $\lim_{T \rightarrow \infty} \mathcal{C}_{ij}(t)$, we require the functions $f_i(s)$, $g_i(s)$, and $h_i(s)$ and their derivatives at the integration endpoints $s = 0, 2, 4, 6$ (0, 1, 3 for the three-spin ring). The relevant quantities are

$$f_1(0) = f_1'(0) = g_1(4) = g_1'(4) = g_1''(4) = 0, \quad (106)$$

$$f_1(2) = g_1(2) = \frac{17}{180}, \quad (107)$$

$$f_1'(2) = g_1'(2) = -\frac{17}{360}, \quad (108)$$

$$f_1''(0) = \frac{2}{9}, \quad (109)$$

$$f_1''(2) = g_1''(2) = -\frac{43}{360}, \quad (110)$$

$$f_1'''(0) = -\frac{3}{16}, \quad (111)$$

$$f_1'''(2) = g_1'''(2) = \frac{21}{80}, \quad (112)$$

$$g_1'''(4) = -\frac{1}{4}, \quad (113)$$

$$f_2(0) = f_2(2) = h_3(6) = h_3'(6) = 0, \quad (114)$$

$$f_2'(0) = \frac{1}{6}, \quad (115)$$

$$f_2'(2) = -\frac{7}{30} + \frac{2}{15} \ln 2, \quad (116)$$

$$f_3(0) = \frac{3739}{7200} - \frac{43}{120} \ln 2, \quad (117)$$

$$f_3(2) = g_3(2) = \frac{7}{15} - \frac{3}{5} \ln 2, \quad (118)$$

$$f_3'(0) = -\frac{1}{4}, \quad (119)$$

$$f_3'(2) = \frac{11}{40} - \frac{29}{30} \ln 2, \quad (120)$$

$$g_3'(2) = \frac{21}{40} - \frac{29}{30} \ln 2, \quad (121)$$

$$g_3(4) = h_3(4) = \frac{69}{1600} + \frac{177}{80} \ln 2 - \frac{459}{320} \ln 3, \quad (122)$$

and

$$g_3'(4) = h_3'(4) = \frac{5}{36} + \frac{57}{20} \ln 2 - \frac{1233}{320} \ln 3. \quad (123)$$

For the three-spin ring, we require

$$f_4(0) = f_4'(0) = g_4(3) = g_4'(3) = 0, \quad (124)$$

$$f_4'(1) = g_4'(1) = \frac{2}{5}, \quad (125)$$

$$f_4''(1) = -\frac{2}{15}, \quad (126)$$

$$g_4''(1) = -\frac{17}{15}, \quad (127)$$

and

$$g_4''(3) = 1. \quad (128)$$

-
- [1] D. Gatteschi, A. Caneschi, L. Pardi, and R. Sessoli, *Science* **265**, 1054 (1994); D. Gatteschi, *Adv. Mater.* **6**, 634 (1994); *Magnetic Molecular Materials*, Vol. 198 of NATO *Advanced Studies Institute, Series E: Applied Sciences*, edited by D. Gatteschi, O. Kahn, J. S. Miller, and F. Palacio (Kluwer Academic, Norwell, MA, 1991).
- [2] J. R. Friedman, M. P. Sarachik, J. Tejada, and R. Ziolo, *Phys. Rev. Lett.* **76**, 3830 (1996); L. Thomas, F. Lonti, R. Allou, D. Gatteschi, R. Sessoli, and B. Barbara, *Nature (London)*, **383**, 145 (1996).
- [3] Y. Furukawa, A. Iwai, K. I. Kumagai, and A. Yakubovsky, *J. Phys. Soc. Jpn.* **65**, 2393 (1996).
- [4] A. Lascialfari, F. Tabak, G. L. Abbati, F. Borsa, M. Corti, and D. Gatteschi, *J. Appl. Phys.* **85**, 4539 (1999).
- [5] A. Müller, J. Meyer, H. Bögge, A. Stammler, and A. Botar, *Chem.-Eur. J* **4**, 1388 (1998).
- [6] D. M. Barnhart, D. L. Clark, J. C. Gordon, J. C. Huffman, J. G. Watkin, and B. D. Zwick, *J. Am. Chem. Soc.* **115**, 8461 (1993).
- [7] A. Bino, D. C. Johnston, D. P. Goshorn, T. R. Talbert, and E. I. Stiefel, *Science* **241**, 1479 (1988); Y. Furukawa, M. Luban, F. Borsa, D. C. Johnston, A. V. Mahajan, L. L. Miller, D. Mentrup, J. Schnack, and A. Bino, *Phys. Rev. B* **61**, 8635 (2000).
- [8] J. S. Gardner, S. R. Dunsiger, B. D. Gaulin, M. J. P. Gingras, J. E. Greedan, R. F. Kiefl, M. D. Lumsden, W. A. MacFarlane, N. P. Raju, J. E. Sonier, I. Swanson, and Z. Tun, *Phys. Rev. Lett.* **82**, 1012 (1999).
- [9] A. L. Barra, A. Caneschi, A. Cornia, F. Fabrizi de Biani, D. Gatteschi, C. Sangregorio, R. Sessoli, and L. Solace, *J. Am. Chem. Soc.* **121**, 5302 (1999).
- [10] A. Bouwen, A. Caneschi, D. Gatteschi, E. Goovaerts, D. Schoemaker, L. Sorace, and M. Stefan, *J. Phys. Chem. B* **105**, 2658 (2001).
- [11] S. Taniguchi, T. Nishikawa, Y. Yasui, Y. Kobayashi, M. Sato, T. Nishioka, M. Kontani, and K. Sano, *J. Phys. Soc. Jpn.* **64**, 2758 (1995); N. Katoh and M. Imada, *J. Phys. Soc. Jpn.* **64**, 4105 (1995).
- [12] A. Lascialfari, D. Gatteschi, F. Borsa, and A. Cornia, *Phys. Rev. B* **55**, 14341 (1997); *ibid.* **56**, 8434 (1997).
- [13] D. Gatteschi, A. Lascialfari, and F. Borsa, *J. Magn. Magn. Mater.* **185**, 238 (1998).
- [14] M.-H. Julien, Z. H. Jang, A. Lascialfari, F. Borsa, M. Horvatic, A. Caneschi, and D. Gatteschi, *Phys. Rev. Lett.* **83**, 227 (1999).
- [15] D. Mentrup, J. Schnack, and M. Luban, *Physica A* **272**, 153 (1999).
- [16] D. Mentrup, H.-J. Schmidt, J. Schnack, and M. Luban, *Physica A* **278**, 214 (2000).
- [17] G. Müller, *Phys. Rev. Lett.* **60**, 2785 (1988).
- [18] R. W. Gerling and D. P. Landau, *Phys. Rev. Lett.* **63**, 812 (1989).
- [19] G. Müller, *Phys. Rev. Lett.* **63**, 813 (1989).
- [20] O. F. de Alcantara Bonfim and G. Reiter, *Phys. Rev. Lett.* **69**, 367 (1992).
- [21] O. Ciftja, M. Luban, M. Auslender, and J. H. Luscombe, *Phys. Rev. B* **60**, 10 122 (1999).
- [22] P. G. deGennes, *J. Phys. Chem. Solids*, **4**, 223 (1958).
- [23] M. Luban, T. Bandos, and O. Ciftja (unpublished).
- [24] C. Schröder, (Ph. D. Thesis, U. Osnabrück, 1998, unpublished), and private communications.
- [25] M. Luban and J. H. Luscombe, *Am. J. Phys.* **67**, 1161 (1999).
- [26] E. W. Montroll, *J. Math. and Phys.* **25**, 37 (1946).